ORBITAL RESONANCES IN THE VINTI SOLUTION

Laura Duffy Zurita
Air Force Institute of Technology, Air Force Research Labs

ABSTRACT

As space becomes more congested, contested, and competitive, high-accuracy orbital predictions become critical for space operations. Current orbit propagators use the two-body solution with perturbations added, which have significant error growth when numerically integrated for long time periods. The Vinti Solution is a more accurate model than the two-body problem because it also accounts for the equatorial bulge of the Earth. Unfortunately, the Vinti solution contains small divisors near orbital resonances in the perturbative terms of the Hamiltonian, which lead to inaccurate orbital predictions. One approach to avoid the small divisors is to apply transformation theory, which is presented in this research. The methodology of this research is to identify the perturbative terms of the Vinti Solution, perform a coordinate transformation, and derive the new equations of motion for the Vinti system near orbital resonances. An analysis of these equations of motion offers insight into the dynamics found near orbital resonances. The analysis in this research focuses on the 2:1 resonance, which includes the Global Positioning System. The phase portrait of a nominal Global Positioning System satellite orbit is found to contain a libration region and a chaotic region. Further analysis shows that the dynamics of the 2:1 resonance affects orbits with semi-major axes ranging from -5.0 to +5.4 kilometers from an exactly 2:1 resonant orbit. Truth orbits of seven Global Positioning System satellites are produced for 10 years. Two of the satellites are found to be outside of the resonance region and three are found to be influenced by the libration dynamics of the resonance. The final satellite is found to be influenced by the chaotic dynamics of the resonance. This research provides a method of avoiding the small divisors found in the perturbative terms of the Vinti Solution near orbital resonances.

INTRODUCTION

Since the launch of the first artificial satellite in 1957, over 39,000 objects have been cataloged as Earth-orbiting satellites. The United States Air Force (USAF) Joint Space Operations Center (JSpOC) is responsible for tracking the locations of these objects [1]. It is crucial to know the location of Earth-orbiting satellites in order to accomplish all space operations including communications, rendezvous, and satellite collision avoidance. In order to precisely predict the future locations of satellites, a highly accurate model that incorporates all aspects of the dynamics of satellite motion is required. Currently, JSpOC uses ground and space based sensors to detect objects in space and uses a simplified general perturbations model, known as Simplified General Perturbations 4 (SGP4), to predict the future locations of these objects [1]. Unfortunately, this method of propagation requires a significant amount of computer processing power and becomes increasingly inaccurate when used for long time periods. SGP4 has error growth of 1-3 km per day, and must be updated frequently with position and velocity information in order to accurately predict satellite locations [2]. SGP4 requires small time steps to make accurate predictions. This is a heavy burden on a numerical integrator and therefore computationally expensive. A better method is needed to accurately and efficiently propagate orbits.

Currently, there are two exactly solvable orbital solutions for motion around the Earth: the two-body solution and the Vinti Solution [3]. Research is currently being conducted at the Air Force Institute of Technology (AFIT) to provide a numerical method for modeling Earth-orbiting objects using the Vinti Solution. Unlike SGP4, which uses the two-body solution and adds the Earth's equatorial bulge as a perturbation, the Vinti Solution accounts for the equatorial bulge in its solution [4, 1]. By accounting for the equatorial bulge, the Vinti Solution numerical orbit propagator is designed to predict satellite locations more accurately than the current two-body solution numerical orbit propagators, such as SGP4. However, a major inaccuracy appears in this numerical solution near orbital resonances.

Orbital resonances occur when the period of an orbit is a rational fraction of the period of the Earth's rotation. The first orbital resonance is the 1:1 resonance, which occurs when the period of the satellite matches the period of the Earth's rotation. This resonance occurs in orbits known as *geosynchronous orbits* (GEO). Geostationary orbits are circular equatorial orbits located in GEO. Geostationary orbits are often utilized by the Air Force for communications and surveillance missions because the satellite stays in the same position above

the Earth as it orbits. The Space Based Infrared System (SBIRS) is a critical Air Force satellite system located in GEO used for "missile early warning, missile defense, battlespace awareness, and technical intelligence mission areas" [5]. SBIRS is one example of the many mission essential satellites located in GEO which require highly accurate position predictions.

Figure 1 shows a two-dimensional representation of various resonant orbits in GEO at the Earth's equator. The x and y axes show the positions of the orbits in kilometers and are located in the equatorial plane of the Earth. *Equatorial orbits* have an inclination of zero degrees. The orbits in Figure 1 are found by first calculating the semi-major axis based on the period of the orbit using equation (1).

$$T = 2\pi\sqrt{\frac{a^3}{\mu}} \tag{1}$$

Where

$$T \equiv \text{orbital period (seconds)}$$

$$a \equiv \text{orbital semi-major axis (km)}$$

$$\mu \equiv \text{Earth's gravitational constant} = 398600.5\ \frac{\text{km}^3}{\text{s}^2}$$

The period of the Earth's rotation used in the calculations equals 23 hours, 56 minutes, and 4.0916 seconds, which is one sidereal day [6]. The period for GEO equals the period of the Earth's rotation, so the semi-major axis for GEO is calculated as approximately 42,164 km. The first orbit has an eccentricity of zero, also known as a *circular orbit*. The rest of the orbits are found by increasing the eccentricity by 0.1 until the orbit reaches an altitude of 160 km at closest approach. At altitudes below 160 km, the effects of atmospheric drag cause satellite to fall to the Earth relatively quickly [7]. Using the above algorithm, 9 orbits are found and shown in Figure 1 with respect to the Earth about its equator. In reality, there are an infinite number of orbits possible within the shown orbits if the eccentricity is not rounded to the nearest tenth decimal place and the inclinations of the orbits are varied. For all of the following figures, the Earth is modeled with a constant radius of 6,378 km.

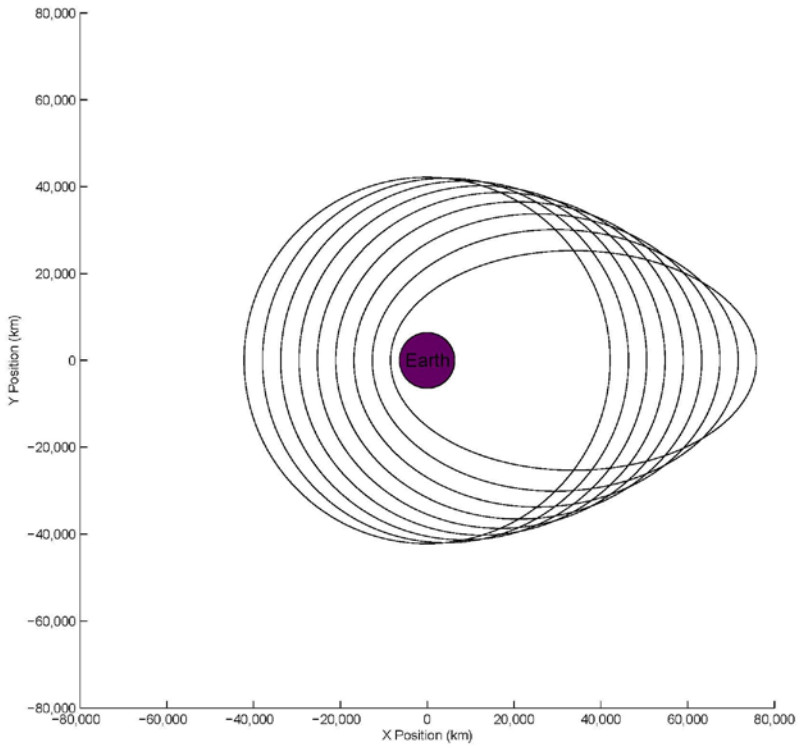

Figure 1. GEO Resonant Orbit

The second orbital resonances occur in medium Earth orbit (MEO), which is defined at altitudes above 2,000 km altitude and below GEO at 35,786 km altitude [8]. The invaluable Global Positioning System (GPS) satellites are located in MEO. To say that GPS satellites are essential to the Air Force is an understatement. GPS satellites are utilized in every facet of U.S. National Security for all missions that require precision positioning or timing [9].

Figure 2 shows various resonant orbits in equatorial MEO. The 1:2 to 1:11 resonant orbits are located in MEO. Satellites in these resonances orbit the Earth 2 to 11 times per day, respectively. The orbits in Figure 2 are found by calculating the semi-major axis based on the period of the desired orbit, which is equal to the period of the Earth's rotation divided by the desired resonance. The periods of these orbits vary between approximately 12 and 2 hours. The semi-major axes of these orbits vary between approximately 26,562 and 8,525 km. The first orbit calculated is a circular orbit and the rest of the orbits are found by increasing the eccentricity by 0.1 until the orbit reaches an altitude of 160 km at closest approach. This process is repeated for the remaining resonances. Using this algorithm, 52 resonant orbits are found in MEO and shown in Figure 2 with respect to the Earth about its equator. In reality, an infinite number of orbits are possible within the shown orbits and at varying inclinations.

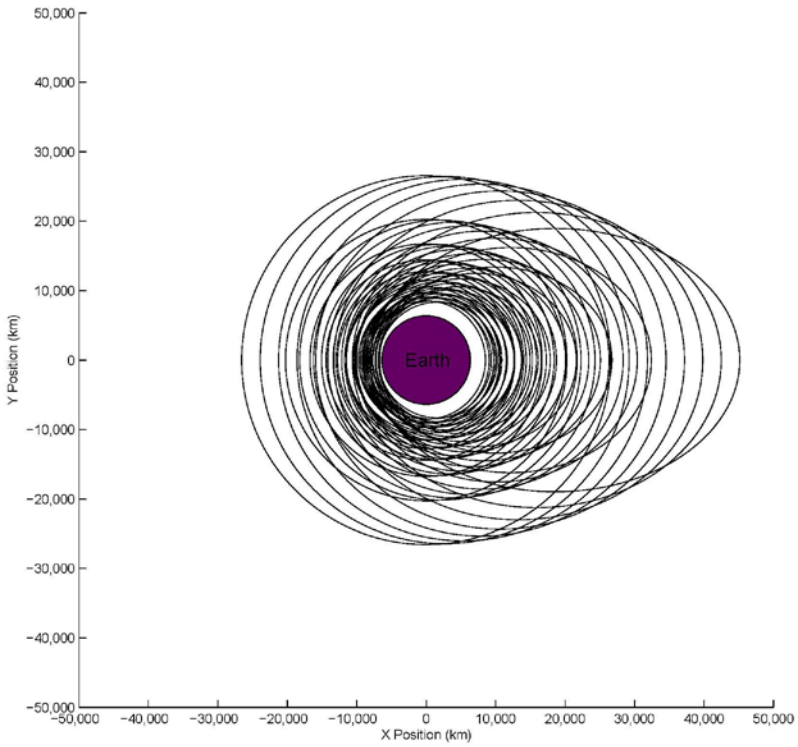

Figure 2. MEO Resonant Orbits

The final orbital resonances about the Earth are the repeating ground-trace orbits located in *low Earth orbit* (LEO), which is any Earth orbit located below an altitude of 2,000 km [7]. The 12:1 to 16:1 resonant orbits are located in LEO. Satellites near these resonances orbit the Earth 12 to 16 times per day, respectively. LEO resonant orbits are utilized for repeating ground trace orbits. One Air Force system that utilizes repeating ground trace orbits is Landsat, which provides ground imagery and can be used for emergency response or disaster relief [10].

Figure 3 shows various resonant orbits in equatorial LEO. The orbits are found by calculating the semi-major axis based on the period of the desired orbit, which is equal to the period of the Earth divided by the desired resonance. The periods of these orbits vary between 120 and 89 minutes. The semi-major axes of these orbits vary between 8,044 and 6,640 km. The first orbit calculated is circular and the rest of the orbits are found by increasing the eccentricity by 0.1 until the orbit reaches an altitude of 160 km at closest approach. This process is repeated for the remaining resonances. Seven resonant orbits are found in LEO using this algorithm and shown in Figure 3 with respect to the Earth about its equator. In reality, an infinite number of orbits are possible within the shown orbits and at varying inclinations.

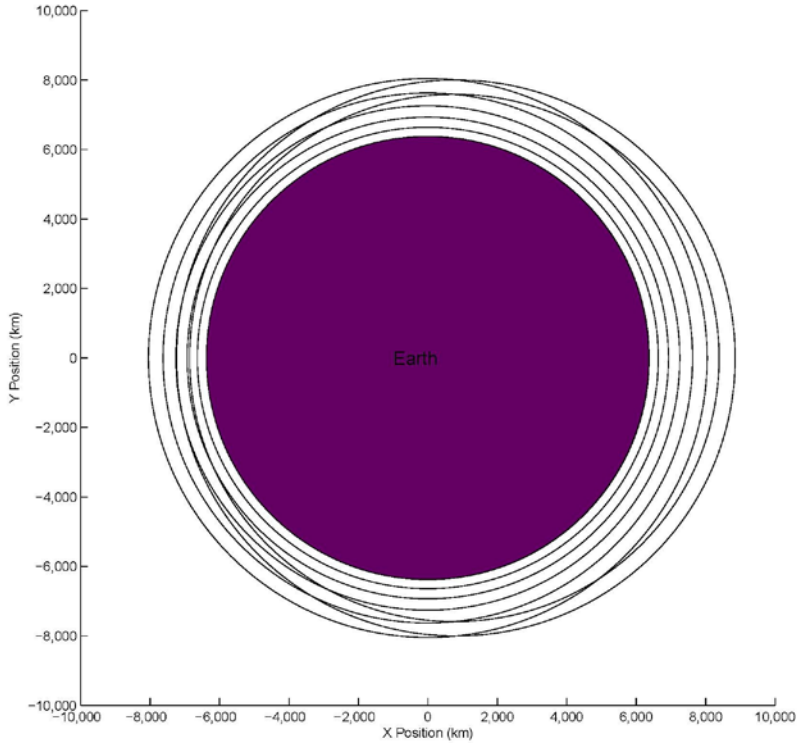

Figure 3. LEO Resonant Orbits

Figures 1-3 show that resonances occur in numerous Earth orbits. Many critical Air Force satellite systems, including SBIRS, GPS, and Landsat, are located in these resonant orbits. Therefore, a more accurate method of predicting the satellites located in resonant orbits is essential for nearly all Air Force missions, and for all operations in space due to the threat of satellite collision. All 68 resonant orbits calculated above are shown to scale in Figure 4.

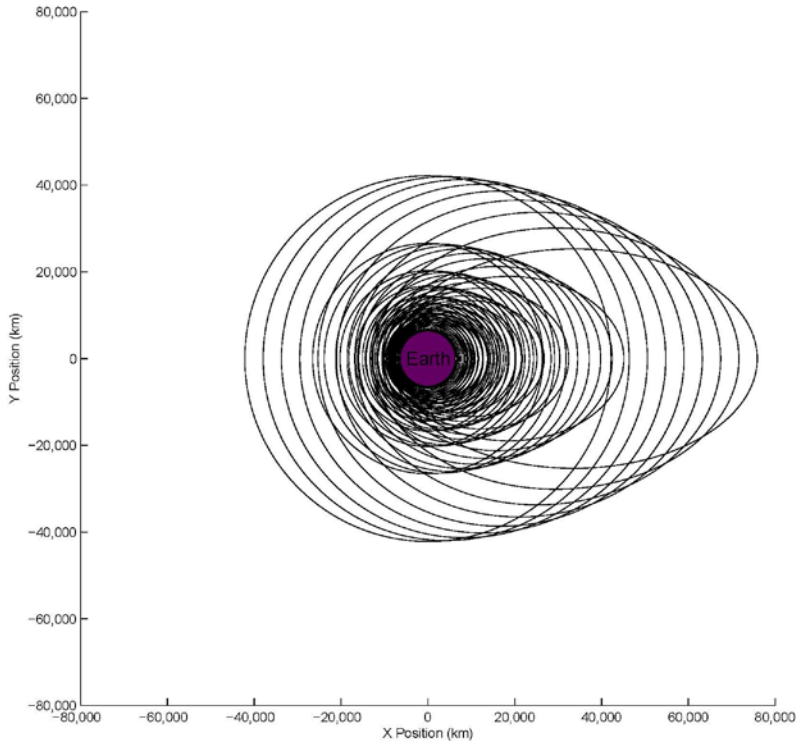

Figure 4. Resonant Orbits

One flaw with the Vinti Solution is that it does not accurately model orbits near resonances. Near resonances, the frequency of the satellite is close to a rational multiple of the frequency of the Earth, which leads to small numbers in the denominators of some of the perturbative terms of the Vinti Solution, known as *small divisors* [11]. Small divisors lead to large perturbation terms in the Vinti Solution. Large perturbation terms directly contradict the fundamental assumption of classical perturbation theory: perturbations must be small. If a satellite is located precisely at an orbital resonance, some perturbations in the Vinti Solution have zeros in the denominator, resulting in terms with values approaching infinity, which are not physically possible and are obviously inaccurate. In order to avoid these large perturbative terms, a modified Vinti Solution must be used near resonances in conjunction with the numerical model for the Vinti Solution. This solution is derived in Chapter III, the Methodology, and is referred to as the *orbital resonance solution*.

Problem Statement

Small divisors in perturbations to the Vinti Solution lead to large, inaccurate terms near orbital resonances about the Earth. These large terms cause incorrect orbital predictions. The research in this thesis provides a solution to avoid the large terms that appear near orbital resonances.

Justification

The research provided in this thesis is necessary in order to predict the locations of Earth-orbiting satellites near orbital resonances using the Vinti Solution. Currently, the orbital propagators used by JSpOC and other space operators are inefficient when used for the thousands of objects located in space and become inaccurate over long time intervals. In order to efficiently communicate with satellites, execute rendezvous operations, and predict satellite collisions, space operators need to use models which accurately and effectively propagate the orbits of their satellites.

The amount of objects orbiting the Earth is constantly increasing. The number of launches per year is growing as the number of space companies and launch sites increases. Also, with a greater number of objects in space, the number of space collisions is increasing. Every collision results in thousands of pieces of orbital debris, which dramatically increases the chance of another collision. The 2007 Chinese antisatellite test

resulted in 3,000 pieces of trackable debris and an estimated 150,000 pieces of debris [12]. In 2009, the Iridium-Cosmos collision resulted in 2,000 pieces of trackable debris and thousands more pieces of debris that are not trackable by JSpOC [12]. For every collision in space, thousands of objects are added to the already large collection of Earth orbiting objects. As this collection increases, the probability of another collision grows considerably. This snowball effect of space collisions will lead to an exponential increase of space debris, drastically decreasing the functionality of space operations near the Earth. Figure 5 shows the past and current effective mass of objects in Earth orbit, as reported by NASA in the January 2015 Orbital Debris Quarterly News [13].

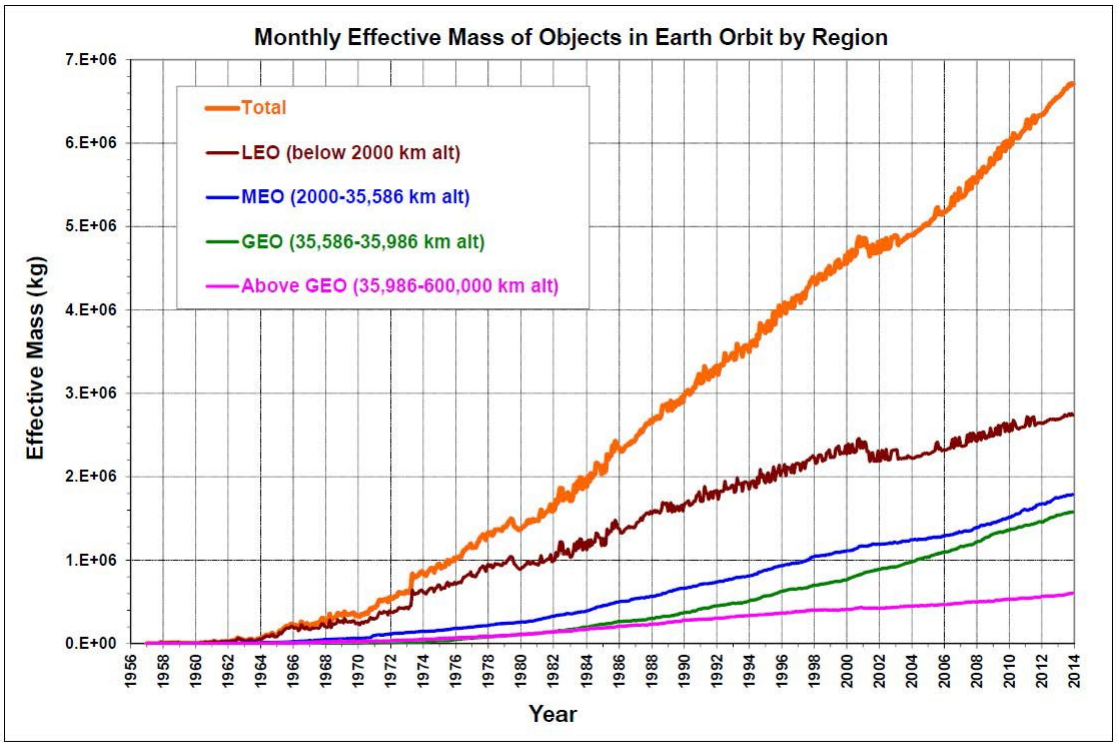

Monthly Effective Mass of Objects in Earth Orbit by Region: This chart displays the mass of all objects in Earth orbit officially cataloged by the U.S. Space Surveillance Network. Divided into orbital altitude regions, "effective mass" accounts for the fraction of its orbit that an object may spend in the different regions.

Figure 5. Monthly Effective Mass of Objects in Earth Orbit by Region, copied from the January 2015 Orbital Debris Quarterly News by NASA [13]

Figure 5 shows that the collection of space objects is already rapidly increasing. This effect must be mitigated in order to allow for the utilization of space in the near future. One way to decrease this number is to accurately and efficiently model the dynamics of objects in space in order to predict and prevent satellite collisions.

The Vinti Solution, when corrected to account for orbital resonances, could provide the accuracy and efficiency needed to predict orbits when performing critical space operations. Unfortunately, numerically modeling the Vinti Solution leads to inaccuracies near orbital resonances. This thesis provides the orbital resonance solution, which is designed to improve the Vinti Solution near resonances. The numerical model of the Vinti Solution plus the orbital resonance solution could increase the precision of orbit predictions and allow for more advanced operations in space.

Assumptions and Limitations

Several assumptions and limitations are made in order to specify the exact problem being solved. The research in this thesis focuses purely on perturbative terms affected by resonances; therefore, all other perturbative terms are assumed to be correctly modeled in the Vinti Solution.

The orbital resonance solution shown in this thesis is implemented and integrated in Matrix

Laboratory (MATLAB). The numerical integrator used in MATLAB for this thesis is ode45: a Runge-Kutta (4,5) formula. Ode45 uses relative and absolute error tolerances to determine the accuracy of the numeric integration [14]. The *absolute error tolerance* of the integrator is defined as the estimated error of the computed value minus the unknown, exact value [15]. The *relative error tolerance* of the integrator is defined as the estimated error of the computed value minus the unknown, exact value divided by the magnitude of that unknown, exact value [15]. The absolute tolerances and relative tolerances used in this thesis are equal to 2.22045×10^{-14}, which is the highest tolerance possible for ode45. Since the solution is computed numerically, it is inherently limited in its accuracy. The integrator and tolerances are chosen in order to maintain high accuracy and reasonable computation times.

Scope and Standards

The research in thesis is restricted in its scope in order to provide a thorough analysis of the orbital resonance solution and the dynamics involved near orbital resonances.

Resonances occur in a variety of manners including third-body resonance, spin- orbit resonances, and orbital resonances due to the gravity field. The orbital resonance solution shown in this thesis deals only with the latter: orbital resonances due to the Earth's gravity field.

Also, the solution shown in this thesis applies exclusively to Earth-orbiting satellites. In order to apply the solution to celestial bodies other than the Earth, the gravitational model of those bodies must be incorporated into the Vinti Solution and the orbital resonance solution.

In Section 1.2, three different types of orbits are mentioned: GEO, MEO, and LEO. This thesis provides the solution for all resonances within these orbital regions, which includes the 1:1 to 16:1 resonances. Beyond the 16:1 resonance, the effects of atmospheric drag are too large to be considered a perturbation, so the Vinti Solution orbit propagator cannot accurately model the dynamics beyond this resonance.

The standards used to evaluate this solution are based on a reference orbit known as the *truth orbit*. Ideally, a truth orbit would use observational data of actual Earth- orbiting satellites. A sufficient amount of real-world satellite data for orbits near resonances is not available to the public. Consequently, a numerical model must be used in order to produce data for the truth orbit. In this thesis, the truth orbit is found using a high-fidelity model developed by Analytical Graphics, Inc.® (AGI) Systems Toolkit® (STK), which is assumed to be close to the value of a true orbit. Data for the truth orbit is produced in STK using the high precision orbit propagator (HPOP) with geopotential terms to order 2 and no other perturbative forces. The integrator used in STK is the Runge-Kutta-Fehlberg (RKF) 7(8) with a relative error of 10^{-13}. The truth orbits produced in STK are used to evaluate the accuracy of the orbital resonance solution. The coordinates produced by STK are translated to Vinti coordinates using a Vinti Solution software package written by Dr. William Wiesel, which numerically integrates the Vinti Solution for a given orbit. The resulting Vinti truth orbit is used to evaluate the accuracy of the orbital resonance solution.

Methodology and Resources

The methodology used to find the orbital resonance solution answers the following investigative questions.

1. Why does the Vinti solution vary drastically near orbital resonances?
2. What method can be used to avoid the inaccuracies near orbital resonances?
3. Does this method provide a solution to accurately model orbits near resonances?

The answers to these questions provide a comprehensive development and analysis of the orbital resonance solution.

The only resources required for this thesis are the computer programs MATLAB, STK, and Vinti Solution software. MATLAB is "a multi-paradigm numerical computing environment and fourth-generation programming language" MATLAB is used for numerical analyses and is used to integrate the differential equations of the orbital resonance solution [15]. STK "is a physics-based software package from Analytical Graphics, Inc.® that allows engineers and scientists to perform complex analyses of ground, sea, air, and space assets, and share results in one integrated solution" [16]. STK is used in this thesis to develop a truth orbit which is used to prove the validity of the orbit resonance solution. The Vinti Solution software is written in C++ and provided

by Dr. Wiesel. It is used to translate orbital coordinates to and from the Vinti system.

LITERATURE REVIEW

The Vinti Solution

The *Vinti Solution* was published in 1959 by John P. Vinti [4, 1]. It is an exactly solvable solution to the motion of satellites around the Earth that accounts for the effects of the Earth's equatorial bulge [17, 1]. The *equatorial bulge* refers to the fact that the radius of the Earth is larger at the equator than at the poles, which causes a large perturbation on satellites. In orbital dynamics, this perturbation is known as J_2. For symmetric planets, the Vinti Solution exactly models orbital motion because the other gravitational terms can be represented as follows [17, 1]:

$$J_4 = -J_2^2$$

$$J_6 = +J_2^3$$

The Vinti Solution is significant because the only other exactly solvable celestial solution found before the Vinti Solution was the solution to the two-body problem. In the *two-body problem*, the equatorial bulge is added as a perturbation and the error in this perturbation grows with time. Perturbations are linearized about the initial time, but as time grows, this linearization becomes more inaccurate, which causes error growth. The Vinti Solution accounts for the equatorial bulge and is a more complete solution for orbital motion around the Earth, allowing for more accurate orbital predictions [17, 1].

Currently, research is being completed at AFIT in order to create an orbit propagator using the Vinti Solution. This propagator is designed to be more accurate than the current two-body problem orbit propagators used by space operators.

A numerical model of the Vinti Solution is ideal for use as a highly accurate orbit propagator, but there are numerical problems which arise near orbital resonances. Near resonances, the frequency of the satellite is close to the frequency of the Earth. Due to the nearly matching frequencies, some of the perturbative terms of the Vinti Solution have small divisors. *Small divisors* lead to large, inaccurate terms in the numerical solution. In this thesis, the terms of the Vinti Solution with small divisors are identified and modified in order to overcome the inaccuracies caused by the resulting large terms. These modified terms, known collectively as the orbital resonance solution, are applied with the numerical model of the Vinti Solution in order to propagate Earth-orbiting satellites.

Orbital Resonances

The issue of orbital resonances was first discovered by French mathematician Jules Henri Poincaré, which he published in Les Methodes Nouvelles de la Mecanique Celeste, Vol II in 1899 [18]. The subject of orbital resonances was explored for the next two centuries by a variety of researchers and astronomers. Most notably, in 1979, Boris Chirikov found highly nonlinear and unstable motion in oscillating systems near resonances [19]. Then in 2010, William Wiesel explored the dynamics caused by orbital resonances in his book *Modern Astrodynamics*. In his research, Wiesel states that *nonlinear resonances* occur in any system when the forcing frequency is a rational multiple of the system frequency. For satellites orbiting the Earth, the forcing frequency is the frequency of the Earth's rotation, which equals one sidereal day [20, 145]. A *sidereal day* is approximately 23 hours, 56 minutes, and 4.0916 seconds [6]. *Orbital resonances* occur when the period of the satellite is a rational fraction of one sidereal day. Rational fractions of the Earth's rotational period occur in satellite motion for the 1:1 to 16:1 resonances. When resonances are greater than 16:1, the semi-major axis of the orbit is so small that effects of atmospheric drag cause perturbation theory techniques to fail. The numerical problem that occurs near orbital resonances is that the frequencies of the satellite and the Earth are close in value, which causes small divisors to appear in the perturbative terms of the Vinti Solution. The terms with small divisors become large and inaccurate in the solution. These large terms directly contradict the fundamental assumption of perturbation theory: perturbations must be small. The terms with small divisors

must be modified to properly model orbits near resonances, which is accomplished in this thesis.
The 1:1 resonance occurs at a commonly used orbit known as GEO. Wiesel explores the effects of orbital resonance in GEO. In his analysis, Wiesel finds the terms that contain the small divisors due to orbital resonances and derives a Hamilto- nian function using these terms. Then, Wiesel performs a canonical transformation and produces the Hamiltonian to model trajectories for geosynchronous orbits. This Hamiltonian is shown in equation (2).

$$H = -\frac{\mu^2}{2(\Lambda_{GEO}+\Phi_{GEO})^2} - \omega_\oplus \Phi_{GEO} - \frac{\mu^4 R_\oplus^2 J_2}{2(\Lambda_{GEO}+\Phi_{GEO})^6} \cdots \\ -\frac{3\mu^4 R_\oplus^2 D_{22}}{(\Lambda_{GEO}+\Phi_{GEO})^6} \sin\left(2\phi_{GEO} + \delta_{22}\right) \tag{2}$$

Where

$$H \equiv \text{Hamiltonian function}$$

$$\omega_\oplus \equiv \text{rotational frequency of the Earth} = 7.2921159 \times 10^{-5} \ \frac{\text{rad}}{\text{s}}$$

$$R_\oplus \equiv \text{radius of Earth} = 6378.135 \text{ km}$$

$$J_2 \equiv \text{second zonal term of Earth's geopotential} = 1.081874 \times 10^{-3}$$

$$D_{22} \equiv \text{sectoral term of Earth's geopotential} = -1.8081 \times 10^{-6}$$

$$\delta_{22} \equiv \text{phase constant} = -60.259^\circ$$

$$\Lambda_{GEO} \equiv \text{axial momentum}$$

$$\Phi_{GEO} \equiv \text{longitudinal momentum}$$

$$\phi_{GEO} \equiv \text{longitudinal coordinate}$$

Using this new Hamiltonian, Wiesel calculates the equations of motion for a satellite in GEO using Hamilton's canonical equations of motion. This process is explained in detail in Section 2.7. The resulting equations of motion are shown in equations (3) and (4).

$$\dot{\Phi}_{GEO} = -\frac{\partial K}{\partial \phi_{GEO}} = \frac{6\mu^4 R_\oplus^2 D_{22}}{(\Lambda_{GEO} + \Phi_{GEO})^6} \cos\left(2\phi_{GEO} + \delta_{22}\right) \tag{3}$$

$$\begin{aligned} \dot{\phi}_{GEO} &= \frac{\partial K}{\partial \Phi_{GEO}} \cdots \\ &= \frac{\mu^2}{(\Lambda_{GEO}+\Phi_{GEO})^3} - \omega_\oplus + \frac{3\mu^4 R_\oplus^2 J_2}{(\Lambda_{GEO}+\Phi_{GEO})^7} + \frac{18\mu^4 R_\oplus^2 D_{22}}{(\Lambda_{GEO}+\Phi_{GEO})^7} \sin\left(2\phi_{GEO} + \delta_{22}\right) \end{aligned} \tag{4}$$

A phase portrait can be produced using these equations of motion, which is useful for analyzing the dynamics of the problem. Figure 6 shows the phase portrait for an equatorial circular orbit in GEO. The trajectories are plotted for a five year time period with initial geocentric longitudes between 0 and 360 degrees and a step size of 5 degrees, so the entire Earth is covered. The x-axis shows the initial longitude of an orbit, and the y-axis shows the momentum associated with the motion in the longitudinal direction.

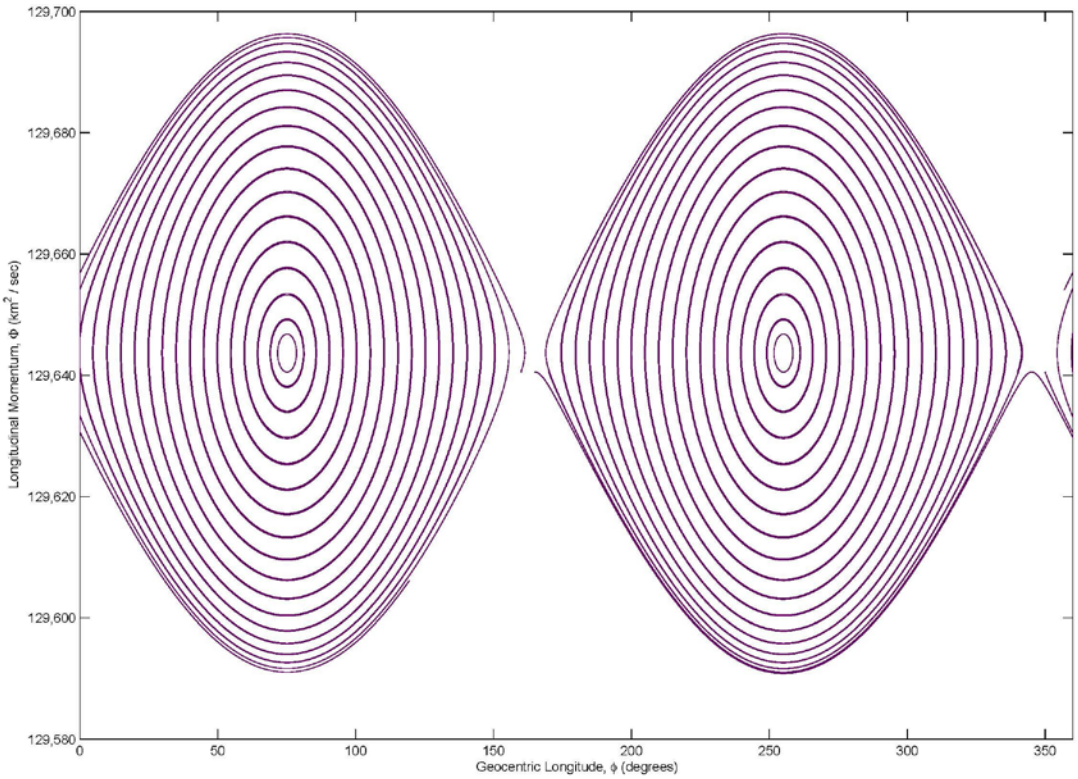

Figure 6. GEO Phase Portrait

Figure 6 can be used to find the four equilibrium points that exist in GEO and to find the maximum change in semi-major axis for an orbit at an equilibrium point.

The two stable, "center," equilibrium points are found in the center of the ovals in Figure 6, at approximate longitudes of 75 and 255 degrees in the phase portrait, which correspond to equatorial locations south of India and south of Mexico. These are known as "libration regions" [20, 148].

The two unstable, "saddle," equilibrium points are located at approximately 165 and 345 degrees longitude in the phase portrait. The regions around the unstable equilibrium points are known as chaotic regions. The unstable equilibrium points are located on the equator northeast of Australia and southwest of Liberia.

By calculating the longitudinal momentum at each time step, the value of the semi-major axis can be found. The semi-major axis is calculated at each time step using the relationship in equation (5). The results of these calculations are plotted in Figure 7 for a time period of five years. For this analysis, longitudes are considered "near" a libration or chaotic region if the initial longitude is within one degree of the equilibrium point.

$$a = \frac{(\Lambda + \Phi)^2}{\mu} \tag{5}$$

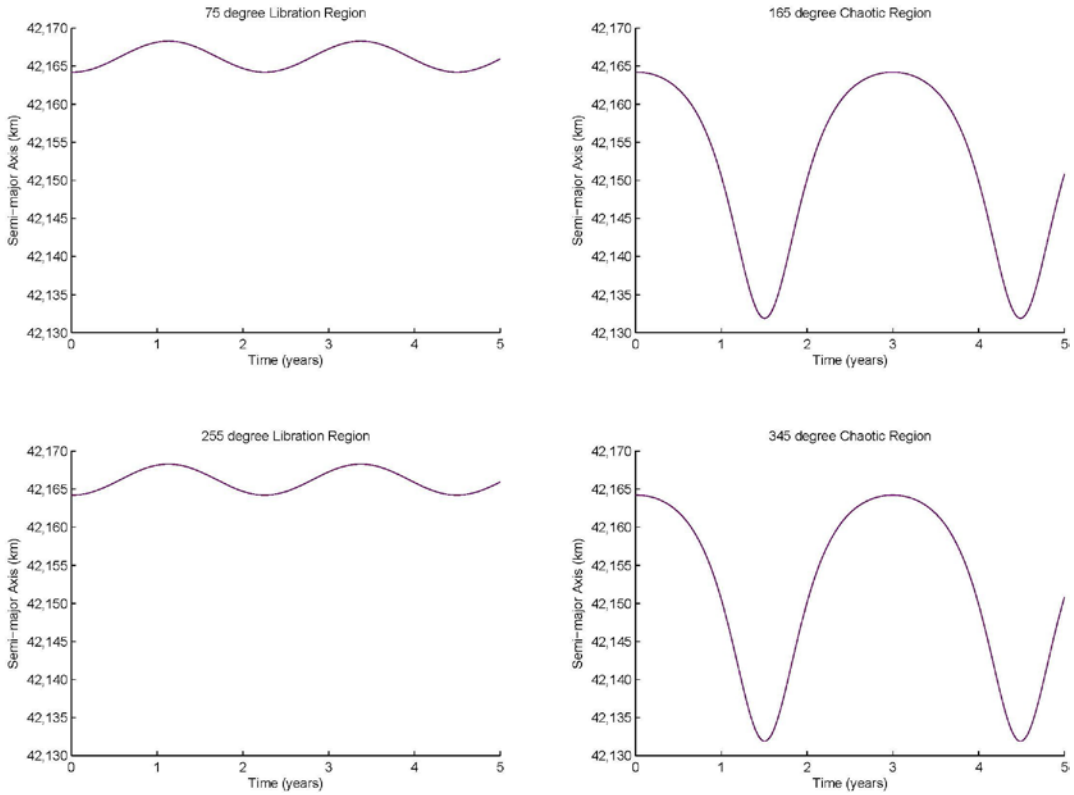

Figure 7. Semimajor Axis of Orbits near Equilibrium Points

The semi-major axis of satellites in libration regions varies up to 4 km, while the semi-major axis of satellites in chaotic regions varies up to 32 km over the five-year time period.

The above phase portrait analysis proves that the dynamics caused by orbital resonances cause satellites to move far from the original, desired position for long time periods. This behavior is detrimental to space operations, where highly accurate location predictions are essential. GPS satellites require highly accurate orbit predictions, but they are located near the 1:2 resonance. Orbiting near a resonance is a major problem due to the dynamics shown in Figures 6 and 7. The dynamics caused by resonances on GPS satellites have been explored by other researchers and the results are presented in Section 2.4.

Resonances in the GPS Constellation

In 2012, researchers in Brazil presented studies on orbits located near the 2:1 resonance [21]. By using canonical transformations, the researchers derived a simplified model of the orbital dynamics near resonances. The phase space of this simplified model was found to resemble the phase space of the simple pendulum [21]. In other words, chaotic motion was found near resonances. In the journal article "Artificial

satellites orbits in 2:1 resonance: GPS constellation," Sampaio, Neto, Fernandes, Moraes, and Terra stated [21]:

> The orbits of synchronous satellites are very complex, from the dynamics point of view. The tesseral harmonics of the geopotential produce multiple resonances which interact resulting [sic] significantly nonlinear motions, when compared to non-resonant orbits. It has been found that the orbital elements show relatively large oscillation amplitudes differing from neighboring trajectories, they are in fact chaotic.

Sampaio, Neto, Fernandes, Moraes, and Terra chose four orbits near the 2:1 resonance and found the change in semi-major axis over time. The results were that the semi-major axis oscillated significantly for all four of the orbits. The smallest oscillation was found to be 3 km and the greatest was 14 km [21]. These results are shown in Figure 8 using the orbital elements in Table 1.

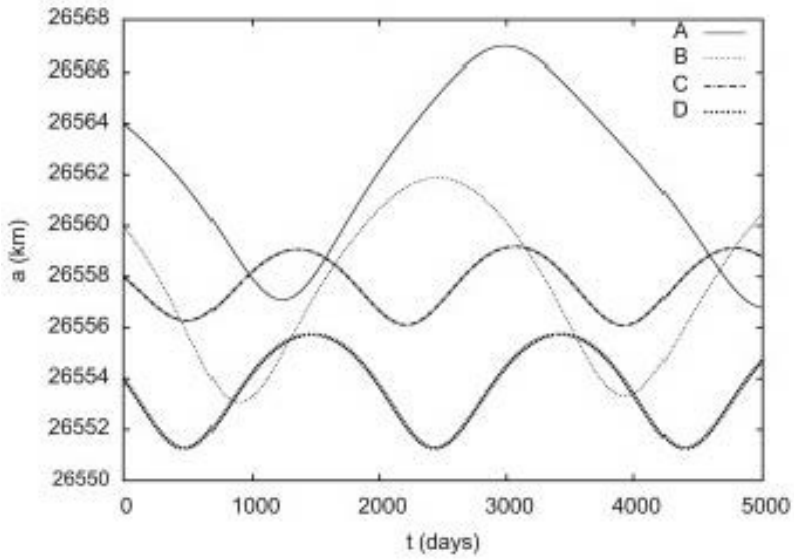

Figure 8. Time Behavior of the Semi-major Axis, copied from "Artificial satellites orbits in 2:1 resonance: GPS constellation" by Sampaio, Neto, Fernandes, Moraes, and Terra [21]

Table 1. Orbital Elements for Figure 8

Point	Semi-major axis (km)	Eccentricity	Inclination (degrees)
A	26,564	0.01	55
B	26,560	0.01	30
C	26,558	0.01	55
D	26,554	0.01	20

Using the above data and performing a study of the phase space of the problem, the researchers reached the following conclusions [21]:

> Inside the region where the resonances are found, the motion can be chaotic, showing sensibility to

initial conditions. Outside the region of junction of the resonances, the orbits are quasi-periodic.

Near resonances, orbits are subject to chaotic dynamics and require highly sensitive equations of motion in order to model numerically. The research in this thesis offers a solution to finding these highly sensitive equations and evaluates the solution.

The quasi-periodicity of orbits outside of resonances is useful in the application of the KAM theorem, presented in Section 2.5.

Orbital Resonances using the KAM Theorem

In 2010, Maj Ralph Bordner attempted to apply the KAM theorem in order to find an analytical method of modeling orbits that would be more accurate than the two-body problem. The KAM theorem was first announced in 1954 by Andrey Kolmogorov and was later rigorously proven by Vladimir Arnol'd and Jurgen Moser, for which it was named the *Kolmogorov-Arnold-Moser* (KAM) theorem [22]. The KAM theorem states that an *n*-degree-of-freedom, integrable Hamiltonian system exists on an *n*-dimensional, invariant deformed torus in phase space, even with small perturbations. Different initial conditions appear on different invariant tori for the same Hamiltonian system [23]. An example of a three-dimensional, unperturbed invariant torus is shown in Figure 9.

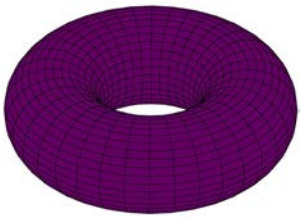

Figure 9. Torus

Bordner proved that the KAM theorem can be accurately applied to model orbits for long time periods as long as there is sufficient data for the orbit, and the orbit is not perturbed by maneuvering the satellite [24, 90]. In other words, the KAM theorem is best used to model orbital debris. However, Bordner found that issues existed in applying the KAM theorem near orbital resonances, specifically the 2:1 resonance used for GPS orbits. When applying the KAM solution to a GPS orbit, Bordner reached the following conclusion [24, 90]:

> It appeared to easily get drawn into finding other local minima rather than the global solution. Hence, the torus found was not 'close' enough for operational use. Thus, until a non-trajectory following method is developed or a way to circumvent the near-commensurability of the peaks is found, the operational GPS mission as we know it cannot benefit from this type of effort either.

Therefore, the mission-critical GPS satellites, which orbit near the 2:1 resonance, cannot be modeled using the KAM theorem: a potentially highly accurate method of modeling orbits.

Bordner describes resonant orbits as having "commensurate frequencies" because the frequency of satellites in resonant orbits have the same frequency or a frequency at a rational multiple of the frequency of the Earth. While presenting his data, Bordner states that "avoiding nearly commensurate frequencies and increasing the number of periods of each basis frequency within the sampled data results in much better reconstruction of the orbital trajectory" [24, 93]. In other words, the KAM theorem could not be applied to resonant orbits because the frequencies of the orbits were not sufficiently irrational. Thus, a method other than the KAM theorem must be applied to orbits near resonances in order to accurately model orbits. The Vinti Solution offers an accurate orbital model. This thesis offers method to avoid the numerical effects of resonances in the Vinti Solution using transformation theory: a subset of classical mechanics explained in Section 2.8.

Classical Orbital Elements

In this thesis, the classical orbital elements are used to define the truth orbits used to validate the orbital resonance solution. The *classical orbital elements* are a set of six scalar values used to describe an orbit in the two body problem [25, 64].

The first classical orbital element is the semimajor axis, *a*, which defines the size of the orbit. It is defined as the length of the longest axis of the orbit [25, 64].

The next element is eccentricity, *e*, which defines the shape of the orbit. Closed orbits are defined with eccentricities between values of 0 and 1 depending on how elliptic the orbit is shaped [25, 64].

The orbital element *i* is the inclination, and it defines the tilt of the orbit relate to the equatorial plane. It is equal to the angle between the normal axis of the equatorial plane and the normal axis of the orbital plane [25, 65].

The right ascension of the ascending node, Ω, defines the position of the ascending node of the orbit. It is equal to the angle between the line of nodes and the vector pointing to the vernal equinox. Vernal equinox is defined as the vector from the Earth to the sun when the sun ascends in the Earth's equatorial orbit on the first day of spring [25, 64-65].

The argument of perigee, ω, defines the position of the point of closest approach of the orbit. It is equal to the angle between the nodal vector and the eccentricity vector [25, 65].

Finally, the true anomaly, *v*, defines the position of the satellite relative to perigee at a given time. It is equal to the angle between the eccentricity vector and the position vector [25, 65].

The classical orbital elements are used in this thesis to define the initial values of the truth orbits in Chapter IV.

Classical Mechanics

Classical mechanics is the study of the motion of interacting bodies, excluding quantum mechanics. It is composed of theories developed by Isaac Newton, Leonhard Euler, Joseph-Louis Lagrange, and William Rowan Hamilton [26, 1]. *Newton's laws of motion* were published in 1687 and provide the foundation for classical mechanics [27, 9]:

> First Law: If there are no forces acting upon a particle, the particle will move in a straight line with constant velocity
>
> Second Law: A particle acted upon by a force moves so that the force vector is equal to the time rate of change of the linear momentum vector
>
> Third Law: When two particles exert forces upon one another, the forces lie along the line joining the particles and the corresponding force vectors are the negative of each other

Newton's laws are used as a basis for *analytical dynamics*, which is a subset of classical mechanics and describes the motion of bodies using scalar functions of kinetic and potential energy [26, 48]. Following Newton, Euler was instrumental in the development of analytical dynamics in the 1700s. He derived the *Euler-Lagrange* equation in 1744, which is shown in equation (6) [26, 152].

$$\frac{\partial f}{\partial y} - \frac{d}{dx}\left(\frac{\partial f}{\partial y'}\right) = 0 \tag{6}$$

Where

$$f \equiv \text{generic function}$$

$$y \equiv \text{y cartesian coordinate}$$

$$x \equiv \text{x cartesian coordinate}$$

This is a partial differential equation that shows the stationary values of a given function, *f*, which is useful for gaining insight into the dynamics of a system. After Euler, Lagrange made the next great development in the field of classical mechanics.

He defined the *Lagrangian function* as an energy-like quantity used to describe a sys- tem in terms of the generalized coordinates, the time rate of change of the generalized coordinates, and time. The Lagrangian is shown in equation (7).

$$L(q_i, \dot{q}_i, t) = T - V \tag{7}$$

Where

$$L \equiv \text{Lagrangian function}$$

$$T \equiv \text{kinetic energy}$$

$$V \equiv \text{potential energy}$$

$$q \equiv \text{generalized coordinate}$$

$$t \equiv \text{time}$$

$$i \equiv \text{counting index} = 1, 2...n$$

$$n \equiv \text{degrees of freedom of the system}$$

Lagrange used this energy-like quantity and the Euler-Lagrange equation to derive Lagrange's equations, which are the equations of motion of a holonomic system and shown in equation (8) [26, 159].

$$\frac{d}{dt}\left(\frac{\partial L}{\partial \dot{q}_i}\right) - \frac{\partial L}{\partial q_i} = 0 \tag{8}$$

These equations result in *n* second-order differential equations of motion, where *n* is the degree of freedom of the system. After Lagrange, Hamilton further developed the field of classical mechanics by deriving a method for finding 2*n* first-order differential equations of motion for a Hamiltonian system. Hamilton defined the *Hamiltonian function*, which is an energy-like quantity used to describe the system in terms of generalized coordinates, generalized momenta, and time [26, 163]. The change in a generalized coordinate with respect to time, also known as the generalized velocity, cannot be appear explicitly in the Hamiltonian function. Once the Hamiltonian is computed using equation (10), the generalized velocities must be eliminated by expressing those quantities in terms of the generalized momenta [26, 163]. The generalized velocities and momenta are related by the kinetic energy of the system, as shown in equation (9) [26, 163].

$$p_i = \frac{\partial L}{\partial \dot{q}_i} \tag{9}$$

Where

$$p \equiv \text{generalized momentum}$$

The Hamiltonian function is shown in equation (10).

$$H(q_i, p_i, t) = \sum_{i=1}^{n} p_i \dot{q}_i - L(q_i, \dot{q}_i, t) \tag{10}$$

Then, the 2*n* equations of motion for the system can be found by computing *Hamilton's canonical equations of motion*, shown in equations (11) and (12) [26, 164].

$$\dot{q}_i = \frac{\partial H}{\partial p_i} \tag{11}$$

$$\dot{p}_i = -\frac{\partial H}{\partial q_i} \tag{12}$$

Equations (11) and (12) are the equations of motion for a Hamiltonian system and describe the dynamics of the system using generalized coordinates, generalized momenta, and time. The generalized coordinates and momenta are represented in the state vector, *x*, and the equations of motion are represented in the dynamics vector, f.

$$\vec{x} = \begin{Bmatrix} q_i \\ p_i \end{Bmatrix}$$

$$\dot{\vec{x}} = \vec{f}(\vec{x}, t) = \begin{Bmatrix} \dot{q}_i \\ \dot{p}_i \end{Bmatrix}$$

The equations of variation for the system are found by linearizing the equations of motion about the initial conditions, shown in equation (13). The equations represented by the vector $\delta \dot{x}$ are linear, time-varying differential equations used to assess the dynamics near a nominal trajectory [20, 6].

$$\delta\dot{\vec{x}} = \frac{\partial \vec{f}}{\partial \vec{x}}\delta\vec{x} = A\delta\vec{x} \tag{13}$$

Where

$$A \equiv \text{partials matrix} = \frac{\partial \vec{f}}{\partial \vec{x}}$$

The linear stability at any point can be determined by calculating the eigenvalues and eigenvectors of the partials matrix at the desired point. Since the partials matrix is a linear model of the system, the eigenvalues and eigenvectors do not give information regarding the stability of the system. The eigenvalues and eigenvectors merely give stability information regarding the point itself. This stability information is useful for gaining insight into the dynamics of the system.

The theories of Newton, Euler, Lagrange, and Hamilton provide the foundation of classical mechanics. Classical mechanics is utilized throughout this thesis for the derivation and analysis of the orbital resonance solution. A subset of classical mechanics is transformation theory and is presented in Section 2.8.

Transformation Theory

Transformation theory describes the process of changing coordinates in Hamiltonian systems [20, 33]. This theory is useful in order to simplify or solve the equations of motion for a system. Wiesel clearly states the concepts of transformation theory in *Modern Astrodynamics, Second Edition*. These concepts are summarized in the algorithm below, which is applied in Chapter III in order to derive the equations for the orbital resonance solution.

First, the old Hamiltonian function is defined in terms of the old coordinates, old momenta, and time.

$$H = H(p_i, q_i, t)$$

Second, the new coordinates and new momenta are defined in order to simplify or solve the equations of motion. They are functions of the old coordinates, old momenta, and time.

$$Q \equiv \text{new generalized coordinate} = Q(p_i, q_i, t)$$

$$P \equiv \text{new generalized momentum} = P(p_i, q_i, t)$$

This step requires significant intuition regarding the dynamics of the problem and some experience with Hamiltonian systems. It is also the most iterative part of transformation theory because if the chosen coordinates are insufficient, then new coordinates must be chosen.

Third, the generating function is created. The algorithm utilized in this thesis uses the F_2 generating function. For explanations of alternative generating functions, reference Chapter 2 of *Modern Astrodynamics, Second Edition*. To generate the F_2 function, the new coordinates and the new momenta are added together. Then, the old coordinates are substituted into the new coordinates. The F_2 function is defined in terms of the old coordinates, new momenta, and time. It is found using equation (14).

$$F_2 = F_2(q_i, P_i, t) = \sum_{i=1}^{n} Q_i P_i \tag{14}$$

Where

$$F_2 \equiv \text{generating function}$$

Fourth, the values of the old momenta and new coordinates are found. The equations for the old momenta are computed by differentiating the generating function with respect to the old coordinates, shown in equation (15). The equations for the new coordinates are computed by differentiating the generating function with respect to the new momenta, shown in equation (16).

$$p_i = \frac{\partial F_2}{\partial q_i} \tag{15}$$

$$Q_i = \frac{\partial F_2}{\partial P_i} \tag{16}$$

Fifth, the new Hamiltonian function is found by differentiating the generating function with respect to time, adding it to the old Hamiltonian, and substituting the new coordinates and new momenta into the new Hamiltonian. This process is shown in equation (17). The new Hamiltonian is a function of the new coordinates, new momenta, and time.

$$K = K(P_i, Q_i, t) = H + \frac{\partial F_2}{\partial t} \tag{17}$$

Where

$$K \equiv \text{new Hamiltonian}$$

Finally, this new Hamiltonian is used to generate the equations of motion for the system. The equations of motion describe the time rate of change of the new coordinates and new momenta. The change in the coordinates with respect to time is equal to the differential of the Hamiltonian with respect to the momenta, shown in equation (18). The change in the momenta with respect to time is equal to the negative of the differential of the Hamiltonian with respect to the coordinates, shown in equation (19).

$$\dot{Q}_i = \frac{\partial K}{\partial P_i} \tag{18}$$

$$\dot{P}_i = -\frac{\partial K}{\partial Q_i} \tag{19}$$

With a clever choice of coordinates, the new equations of motion will be simpler than the old equations of motion and may even be solvable [20, 33-42]. The above algorithm for changing coordinates using transformation theory is applied in Chapter III to derive the equations for the orbital resonance solution.

METHODOLOGY

The Vinti System

Near resonances, the Vinti Solution fails due to small divisors in some of the perturbative terms. The terms with the small divisors are identified and provided in equation (20) along with the local action angle coordinates from the Vinti system. This Hamiltonian function describes the motion of the Vinti system near orbital resonances in terms of the old Vinti coordinates and momenta.

$$H = \sum_{\alpha=1}^{3}\sum_{\beta=1}^{3} \Omega_\alpha (I_\alpha - I_{\alpha 0}) + \frac{1}{2}\frac{\partial \Omega_\alpha}{\partial I_\beta}(I_\alpha - I_{\alpha 0})(I_\beta - I_{\beta 0}) \cdots \\ + C_n \cos(\vec{j} \cdot \vec{\theta}) + S_n \sin(\vec{j} \cdot \vec{\theta}) \tag{20}$$

Where

$\Omega \equiv$ frequency variable

$I \equiv$ action variable

$I_0 \equiv$ initial value of action variable

$C_n \equiv$ gravity model cosine coefficient

$S_n \equiv$ gravity model sine coefficient

$\vec{j} = \langle j_1, j_2, j_3 \rangle$

$j \equiv$ resonance variable

$\vec{\theta} = \langle \theta_1, \theta_2, \theta_3 \rangle$

$\theta \equiv$ angle variable

The three frequencies of the Vinti system are known as the anomalistic frequency, the Earth's rotational frequency combined with the nodal regression rate, and the apsidal regression rate. The anomalistic frequency is approximately the mean motion including the effects due to the equatorial bulge [24, 47]. Bordner shows that this can be approximately calculated using equation (21).

$$\Omega_1 = \frac{d\theta_1}{dt} \approx \sqrt{\frac{\mu}{a^3}}\left(1 - \frac{3J_2R_\oplus^2}{2a^2(1-e^2)^{\frac{3}{2}}}\left(\frac{3}{2}\sin i^2 - 1\right)\right) \tag{21}$$

Where

$$\Omega_1 \equiv \text{anomalistic frequency}$$

$$\theta_1 \equiv \text{mean anomaly}$$

$$e \equiv \text{orbital eccentricity}$$

$$i \equiv \text{orbital inclination}$$

The second frequency, the Earth's rotational frequency plus nodal regression rate, is the frequency that the orbit precesses in the rotating frame due to the equatorial bulge [24, 47]. The second frequency can be approximately calculated using equation (22).

$$\Omega_2 = \frac{d\theta_2}{dt} \approx \omega_\oplus + \frac{3\sqrt{\mu} J_2 R_\oplus^2}{2a^{\frac{7}{2}}(1-e^2)^2} \cos i \tag{22}$$

Where

$$\Omega_2 \equiv \text{Earth's rotation plus nodal regression rate}$$

$$\theta_2 \equiv \text{longitude of the ascending node}$$

The third frequency, the apsidal regression rate, is the regression of the line of apsides due to the non-circular shape of the orbit [24, 48]. The third frequency can be approximately calculated using equation (23).

$$\Omega_3 = \frac{d\theta_3}{dt} \approx -\frac{3\sqrt{\mu} J_2 R_\oplus^2}{2a^{\frac{7}{2}}(1-e^2)^2} \left(\frac{5}{2} \sin i^2 - 2 \right) \tag{23}$$

Where

$$\Omega_3 \equiv \text{apsidal regression rate}$$

$$\theta_3 \equiv \text{argument of perigee}$$

The above variables and Hamiltonian must be modified using a canonical trans- formation to derive the orbital resonance solution.

Transformation Theory Application

Transformation theory is applied to the old Hamiltonian of the Vinti System near orbital resonances. All of the coordinates and momenta used in this transformation are defined below.

$$\begin{Bmatrix} \theta_1 \\ \theta_2 \\ \theta_3 \end{Bmatrix} \equiv \text{generalized coordinates of the Vinti System}$$

$$\begin{Bmatrix} I_1 \\ I_2 \\ I_3 \end{Bmatrix} \equiv \text{generalized momenta of the Vinti System}$$

$$\begin{Bmatrix} \phi_1 \\ \phi_2 \\ \phi_3 \end{Bmatrix} \equiv \text{generalized coordinates of the orbital resonance solution}$$

$$\begin{Bmatrix} \Phi_1 \\ \Phi_2 \\ \Phi_3 \end{Bmatrix} \equiv \text{generalized momenta of the orbital resonance solution}$$

In the old Hamiltonian, the "$j \cdot \theta$" term is the *resonant term*. The resonant term results in the small divisors found near resonances in the Vinti Solution. The resonant term is the focus of this transformation. In fact, the new coordinates are chosen so that one of them becomes this resonant term. After a few iterations using various coordinates, the new coordinates are chosen and defined in equations (24), (25), and (26).

$$\phi_1 = \vec{j} \cdot \vec{\theta} = j_1\theta_1 + j_2\theta_2 + j_3\theta_3 \tag{24}$$

$$\phi_2 = \theta_1 \tag{25}$$

$$\phi_3 = \theta_2 \tag{26}$$

Next, using equation (14), the generating function is calculated and shown in equation (27).

$$F_2 = \sum_{i=1}^{n} \phi_i \Phi_i = \Phi_1(j_1\theta_1 + j_2\theta_2 + j_3\theta_3) + \Phi_2\theta_1 + \Phi_3\theta_2 \tag{27}$$

Then, using equation (15), the expressions of the old momenta are calculated and shown in equations (28), (29), and (30).

$$\frac{\partial}{\partial q}$$

$$I_1 = \frac{\partial F_2}{\partial \theta_1} = \Phi_1 j_1 + \Phi_2 \tag{28}$$

$$I_2 = \frac{\partial F_2}{\partial \theta_2} = \Phi_1 j_2 + \Phi_3 \tag{29}$$

$$I_3 = \frac{\partial F_2}{\partial \theta_3} = \Phi_1 j_3 \tag{30}$$

Next, the expressions for the old momenta are inverted in order to solve for the new momenta. Equations (31), (32), and (33) show the expressions for the new momenta.

$$\Phi_1 = \frac{I_3}{j_3} \tag{31}$$

$$\Phi_2 = I_1 - \frac{I_3 j_1}{j_3} \tag{32}$$

$$\Phi_3 = I_2 - \frac{I_3 j_2}{j_3} \tag{33}$$

Next, using equation (17), and substituting equations (28), (29), and (30) into the old Hamiltonian, the new Hamiltonian is calculated and shown in equation (34).

$$K = \sum_{\alpha=1}^{3}\sum_{\beta=1}^{3} \Omega_\alpha(\Phi-\Phi_0)'_\alpha + \frac{1}{2}\frac{\partial\Omega_\alpha}{\partial\Phi_\beta}(\Phi-\Phi_0)'_\alpha(\Phi-\Phi_0)'_\beta \cdots + C_n\cos(\phi_1) + S_n\sin(\phi_1) \tag{34}$$

Where

$$(\Phi-\Phi_0)' = \begin{Bmatrix} \Phi_1 j_1 + \Phi_2 - \Phi_{10} j_1 - \Phi_{20} \\ \Phi_1 j_2 + \Phi_3 - \Phi_{10} j_2 - \Phi_{30} \\ \Phi_1 j_3 - \Phi_{10} j_3 \end{Bmatrix}$$

$$\frac{\partial\Omega}{\partial\Phi} = \begin{Bmatrix} \frac{\partial\Omega_1}{\partial I_1} & \frac{\partial\Omega_1}{\partial I_2} & \frac{\partial\Omega_1}{\partial I_3} \\ \frac{\partial\Omega_2}{\partial I_1} & \frac{\partial\Omega_2}{\partial I_2} & \frac{\partial\Omega_2}{\partial I_3} \\ \frac{\partial\Omega_3}{\partial I_1} & \frac{\partial\Omega_3}{\partial I_2} & \frac{\partial\Omega_3}{\partial I_3} \end{Bmatrix}$$

The Orbital Resonance Solution

The new Hamiltonian shown in equation (34) is used to find the equations of motion for the Vinti system near resonances. By applying equation (18), and equation (19) the equations of motion are found by differentiating using the relationships shown in equations (35) and (36).

$$\dot{\phi}_i = \frac{\partial K}{\partial\Phi_i} \tag{35}$$

$$\dot{\Phi}_i = -\frac{\partial K}{\partial\phi_i} \tag{36}$$

After differentiating the new Hamiltonian with respect to the coordinates and momenta, the six equations of motion for the orbital resonance solution are found. The new Hamiltonian does not contain the coordinates $\varphi 2$ or $\varphi 3$; therefore, the conjugate momenta of these coordinates are constant for all time. The final equations of motion of the orbital resonance solution are shown in equations (37)-(42).

$$\dot{\phi}_1(t) = \sum_{\alpha=1}^{3}\sum_{\beta=1}^{3} j_\alpha \Omega_\alpha + \frac{\partial \Omega_\alpha}{\partial \Phi_\beta} j_\beta (\Phi - \Phi_0)'_\alpha \tag{37}$$

$$\dot{\phi}_2(t) = \sum_{\alpha=1}^{3} \Omega_1 + \frac{\partial \Omega_1}{\partial \Phi_\alpha} (\Phi - \Phi_0)'_\alpha \tag{38}$$

$$\dot{\phi}_3(t) = \sum_{\alpha=1}^{3} \Omega_2 + \frac{\partial \Omega_2}{\partial \Phi_\alpha} (\Phi - \Phi_0)'_\alpha \tag{39}$$

$$\dot{\Phi}_1(t) = C_n \sin(\phi_1) - S_n \cos(\phi_1) \tag{40}$$

$$\dot{\Phi}_2(t) = 0 \tag{41}$$

$$\dot{\Phi}_3(t) = 0 \tag{42}$$

Equations (37)-(42) are the equations of motion for the orbital resonance solution of the Vinti system.

RESULTS AND ANALYSIS

GPS Orbital Parameters

First, the coordinates and momenta of a nominal GPS orbit are found. These variables are found using Vinti Solution software provided by Wiesel. The software takes the Cartesian position and velocity coordinates of an orbit at any point, uses a numerical model of the Vinti Solution, and outputs the coordinates and momenta of the orbit in terms of the Vinti system.

The orbital elements defining a nominal GPS orbit are found in the Global Positioning System Standard Positioning Service Performance Standard and are listed below [28].

$$a_{GPS} = \text{GPS orbit semi-major axis} = 26559.710 \text{ km}$$

$$i_{GPS} = \text{GPS orbit inclination} = 55^\circ$$

These orbital elements are converted to Cartesian coordinates in non-dimensional distance units, DU, and non-dimensional velocity units using equations (43) and (44).

$$\begin{Bmatrix} x \\ y \\ z \end{Bmatrix} = \begin{Bmatrix} \frac{a(1-e)}{R_\oplus} \\ 0 \\ 0 \end{Bmatrix} \tag{43}$$

$$\begin{Bmatrix} \dot{x} \\ \dot{y} \\ \dot{z} \end{Bmatrix} = \begin{Bmatrix} 0 \\ \sqrt{2\left(\frac{R_\oplus}{a(1-e)} - \frac{R_\oplus}{2a}\right)}\cos i \\ \sqrt{2\left(\frac{R_\oplus}{a(1-e)} - \frac{R_\oplus}{2a}\right)}\sin i \end{Bmatrix} \tag{44}$$

Where

$$x, y, z \equiv \text{Cartesian position coordinates (nondimensional distance units)}$$

The values of the calculated coordinates for the nominal GPS orbit are listed below. The coordinates are calculated in nondimensional distance units and the velocities are calculated in nondimensional distance units per time units.

$$\begin{Bmatrix} x \\ y \\ z \end{Bmatrix} = \begin{Bmatrix} 4.164181 \text{ (DU)} \\ 0 \\ 0 \end{Bmatrix}$$

$$\begin{Bmatrix} \dot{x} \\ \dot{y} \\ \dot{z} \end{Bmatrix} = \begin{Bmatrix} 0 \\ 0.281078 \ \frac{\text{DU}}{\text{TU}} \\ 0.401421 \ \frac{\text{DU}}{\text{TU}} \end{Bmatrix}$$

After inputting the above coordinates into the Vinti Solution software, the variables of the resonance Hamiltonian are output. The values for the coordinates, momenta, frequencies, partials, and gravity model coefficients calculated in the Vinti Solution software are provided below.

$$\begin{Bmatrix} \theta_1 \\ \theta_2 \\ \theta_3 \end{Bmatrix} = \begin{Bmatrix} 3.14115254212883 \\ 1.57079628270754 \\ -4.40834029280524 \times 10^{-8} \end{Bmatrix}$$

$$\begin{Bmatrix} I_1 \\ I_2 \\ I_3 \end{Bmatrix} = \begin{Bmatrix} 2.55961607247161 \times 10^{-9} \\ 8.70110419770256 \times 10^{-1} \\ 1.17045966711800 \end{Bmatrix}$$

$$\begin{Bmatrix} \Omega_1 \\ \Omega_2 \\ \Omega_3 \end{Bmatrix} = \begin{Bmatrix} 1.17691524082448 \times 10^{-1} \\ 1.17695078871764 \times 10^{-1} \\ 5.88551639511689 \times 10^{-2} \end{Bmatrix}$$

$$\frac{\partial \Omega}{\partial I} = \begin{Bmatrix} -.173027367744446 & -.173032609369944 & -.173023313481916 \\ -.173032579478445 & -.173053690186322 & -.173028900086754 \\ -.173023283592948 & -.173028900086512 & -.173009514095713 \end{Bmatrix}$$

$$C_n = 1.863845985594790 \times 10^{-9}$$

$$S_n = 1.261360044523120 \times 10^{-9}$$

The period of a GPS orbit is calculated as approximately 43, 077 seconds, or 12 hours, while the rotational period of the Earth is approximately 86, 164 seconds, or 24 hours. The rotational period of the Earth divided by the period of the GPS orbit is approximately 2.0002, which means that the GPS orbit is very near the 2:1 resonance. The resonance vector for a 2:1 resonant orbit is defined below.

$$\vec{j}_{GPS} = \begin{Bmatrix} 0 \\ 1 \\ -2 \end{Bmatrix}$$

Next, a change of variables is completed using equations (24)-(26) and (31)-(33) from the coordinate transformation. The new coordinates and new momenta are calculated and provided below.

$$\phi_1 = j_1\theta_1 + j_2\theta_2 + j_3\theta_3 = 1.5707963708743 46$$

$$\phi_2 = \theta_1 = 3.141152542128830$$

$$\phi_3 = \theta_2 = 1.570796282707540$$

$$\Phi_1 = \frac{I_3}{j_3} = -0.585229833559000$$

$$\Phi_2 = I_1 - \frac{I_3 j_1}{j_3} = 2.559616072471610 \times 10^{-9}$$

$$\Phi_3 = I_2 - \frac{I_3 j_2}{j_3} = 1.455340253329256$$

All of the variables used in the orbital resonance solution are shown above. Trajectories of the GPS orbit can be calculated by numerically integrating the differential equations of the orbital resonance solution using the above variables.

One Degree of Freedom Orbital Resonance Solution

In order to analyze the dynamics due to orbital resonances, the system is reduced to a one degree of freedom system. The coordinate is $\varphi 1$, the resonant term, and the momentum is $\Phi 1$, the associated momentum of the resonant term. This is a valid simplification because the $\Phi 2$ and $\Phi 3$ momenta are constant in the orbital resonance solution and $\varphi 2$ and $\varphi 3$ coordinates do not affect the dynamics due to resonance. The $\varphi 2$, $\varphi 3$, $\Phi 2$, and $\Phi 3$ variables of the orbital resonance solution are set to zero, resulting in the equations of motion for a one degree of freedom system.

By equating the $\varphi 2$, $\varphi 3$, $\Phi 2$, and $\Phi 3$ variables to zero in equation (40), the equation of motion of the momentum, $\Phi 1$, for a one degree of freedom system is found and shown below.

$$\dot{\Phi}_1(t) = C_n \sin\phi_1 - S_n \cos\phi_1$$

This equation can be further simplified by changing variables to a harmonic amplitude and phase representation by using equations (45) and (46).

$$C_n = D_n \cos\delta \tag{45}$$

$$S_n = -D_n \sin\delta \tag{46}$$

Where

$$D_n \equiv \text{harmonic amplitude}$$

$$\delta \equiv \text{harmonic phase}$$

The C_n and S_n variables are substituted by the harmonic amplitude and phase variables, and the resulting momentum equation of motion is shown below.

$$\dot{\Phi}_1(t) = D_n \cos\delta \sin\phi_1 + D_n \sin\delta \cos\phi_1$$

Using the trigonometric identity $\sin(x+y) = \sin x \cos y + \cos x \sin y$, the one degree of freedom equation of motion for the momentum is simplified and its final form is shown in equation (47).

$$\dot{\Phi}_1(t) = D_n \sin(\phi_1 + \delta) \tag{47}$$

By equating the φ_2, φ_3, Φ_2, and Φ_3 variables to zero in equation (37), the one degree of freedom equation of motion for the coordinate φ_1 is found and shown in equation (48).

$$\begin{aligned}\dot{\phi}_1(t) &= \Omega_1 j_1 + \Omega_2 j_2 + \Omega_3 j_3 \cdots \\ &+ \left(\frac{\partial \Omega_1}{\partial I_1} j_1^2 + \frac{\partial \Omega_2}{\partial I_2} j_2^2 + \frac{\partial \Omega_3}{\partial I_3} j_3^2 + 2\frac{\partial \Omega_1}{\partial I_2} j_1 j_2 + 2\frac{\partial \Omega_1}{\partial I_3} j_1 j_3 + 2\frac{\partial \Omega_2}{\partial I_3} j_2 j_3 \right)(\Phi_1 - \Phi_{10})\end{aligned} \tag{48}$$

Equations (47) and (48) are the one degree of freedom equations of motion of the orbital resonance solution. They are used to analyze the dynamics caused by orbital resonance.

GPS Orbit Equilibrium Points

Next, the equilibrium points of the GPS orbit are found by setting $\dot{\varphi}_1$ and $\dot{\Phi}_1$ in equations (47) and (48) equal to zero. The equilibrium points occur at the points corresponding to the values of $\delta\Phi_1$ and φ_1 shown in equations (49) and (50). There exists only one equilibrium value of $\delta\Phi_1$ for a given system. Multiple equilibrium values of φ_1 can exist for a given system, as long as they are within the bounds of 0° and 360°.

$$\delta\Phi_1 = (\Phi_1 - \Phi_{10}) = -\frac{\Omega_1 j_1 + \Omega_2 j_2 + \Omega_3 j_3}{\frac{\partial\Omega_1}{\partial I_1} j_1^2 + \frac{\partial\Omega_2}{\partial I_2} j_2^2 + \frac{\partial\Omega_3}{\partial I_3} j_3^2 + 2\frac{\partial\Omega_1}{\partial I_2} j_1 j_2 + 2\frac{\partial\Omega_1}{\partial I_3} j_1 j_3 + 2\frac{\partial\Omega_2}{\partial I_3} j_2 j_3} \tag{49}$$

$$\phi_1 = N\pi + \delta \tag{50}$$

Where

$$N \equiv \text{integer counting variable} = 0, 1, 2, ...$$

$$0^\circ \leq \phi_1 \leq 360^\circ$$

Within the values of 0◦ and 360◦, two equilibrium points are found for the nominal GPS orbit. The values of the equilibrium points are shown below. The x-component of the equilibrium point is φ_1, and the y-component of the equilibrium point is $\delta\Phi_1$.

$$P_1 \equiv \text{first equilibrium point}$$

$$= (34.088224904562992^\circ, -8.815684073697417 \times 10^{-5})$$

$$P_2 \equiv \text{second equilibrium point}$$

$$= (214.0882249045630^\circ, -8.815684073697417 \times 10^{-5})$$

In order to analyze the stability of these points, the partials matrix is found using equation (13). The resulting partials matrix for the linearized one degree of freedom equations of motion is shown below in equation (51).

$$A = \begin{Bmatrix} \frac{\partial\dot{\phi}_1}{\partial\phi_1} & \frac{\partial\dot{\phi}_1}{\partial\Phi_1} \\ \frac{\partial\dot{\Phi}_1}{\partial\phi_1} & \frac{\partial\dot{\Phi}_1}{\partial\Phi_1} \end{Bmatrix} =$$

$$\begin{Bmatrix} 0 & \frac{\partial\Omega_1}{\partial I_1} j_1^2 + \frac{\partial\Omega_2}{\partial I_2} j_2^2 + \frac{\partial\Omega_3}{\partial I_3} j_3^2 + 2\frac{\partial\Omega_1}{\partial I_2} j_1 j_2 + 2\frac{\partial\Omega_1}{\partial I_3} j_1 j_3 + 2\frac{\partial\Omega_2}{\partial I_3} j_2 j_3 \\ D_n \cos(\delta + \phi_1) & 0 \end{Bmatrix} \tag{51}$$

The stability of the equilibrium points can be assessed by computing the eigenvalues of the partials matrix at P_1 and P_2. Each equilibrium point has two eigenvalues since the partials matrix is a 2×2 matrix. The values of these eigenvalues are listed below.

$$\lambda_{P_1} = \pm 0.197304468450755 \times 10^{-4} i$$

$$\lambda_{P_2} = \pm 0.197304468450755 \times 10^{-4}$$

Where

$$\lambda \equiv \text{eigenvalue}$$

P_1 is classified as a marginally stable, "center," equilibrium point because both eigenvalues lie on the imaginary axis and are non-repeating. P_2 is classified as an unstable, "saddle," equilibrium point because one eigenvalue is positive on the real axis and therefore unstable, while the other eigenvalue is negative on the real axis and therefore stable. These equilibrium points repeat in a center - saddle pattern as $\varphi 1$ increases. The only equilibrium points that require analysis are the two listed above that reside within the range of $0^\circ \leq \varphi 1 \leq 360^\circ$.

The frequency of the one degree of freedom system is found in the imaginary component of the marginally stable eigenvalue $\lambda P1$. The frequency is equal to 0.197304468450755×TU. When converted back to dimensional units, this means that the frequency is 44.186983462275663 degrees/TU. Since the frequency of the system is very low, the orbits must be analyzed for long time periods in order to observe the system dynamics due to resonance. Unfortunately, integrating for long time periods introduces the problem of numerical errors due to rounding tolerances.

GPS Orbit Equations of Variation

The equations of variation are used to assess the linear dynamics in the vicinity of a designated point. The equations of variation of the orbital resonance solution are found using equation (13), $\dot{\delta x}=A\delta x$, and are shown in equation (52).

$$\begin{Bmatrix} \delta\dot{\phi}_1 \\ \delta\dot{\Phi}_1 \end{Bmatrix} = A \begin{Bmatrix} \delta\phi_1 \\ \delta\Phi_1 \end{Bmatrix} =$$

$$\begin{Bmatrix} 0 & \frac{\partial\Omega_1}{\partial I_1} j_1^2 + \frac{\partial\Omega_2}{\partial I_2} j_2^2 + \frac{\partial\Omega_3}{\partial I_3} j_3^2 + 2\frac{\partial\Omega_1}{\partial I_2} j_1 j_2 + 2\frac{\partial\Omega_1}{\partial I_3} j_1 j_3 + 2\frac{\partial\Omega_2}{\partial I_3} j_2 j_3 \\ D_n \cos(\delta + \phi_1) & 0 \end{Bmatrix} \begin{Bmatrix} \delta\phi_1 \\ \delta\Phi_1 \end{Bmatrix} \quad (52)$$

The trajectories of the phase space are computed by numerically integrating the equations of variation in MATLAB. The phase portrait of the linearized one degree of freedom system orbital resonance solution near the center equilibrium point is found by numerically integrating equation (52) with initial conditions at P1 for a time period of 0 to 106 TU. Then, the value of $\delta\varphi 1$ is varied from 0° to 45° with a step size of 1°. This phase portrait is shown in Figure 10.

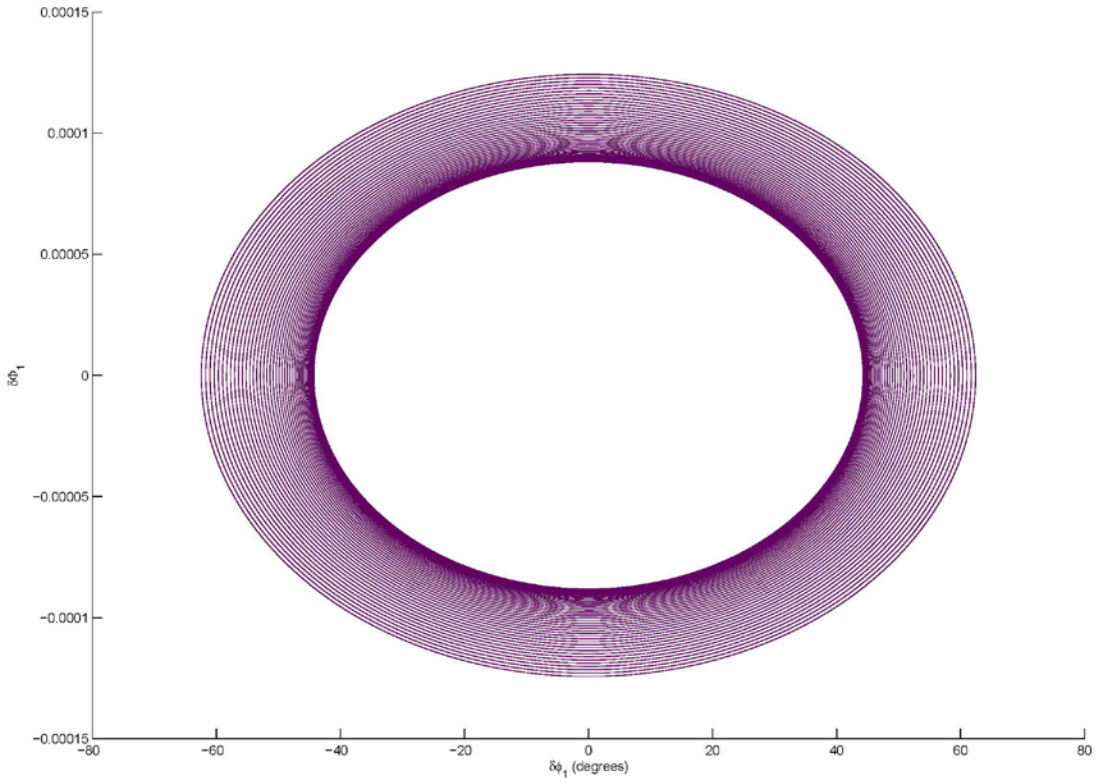

Figure 10. Equations of Variation about the Center Equilibrium Point Phase Portrait

The direction of motion of all the above trajectories is counterclockwise. The displacement along the $\delta\Phi 1$ axis for the trajectory calculated at the center equilibrium point is equal to twice the value of δΦ1 of the center equilibrium point, which is computed as $1.76313681474 \times 10{-}4$. The trajectory closest to the center of Figure 10 shows the linear dynamics at the center equilibrium point. In Figure 10, the trajectories closest to the center equilibrium point appear close to each other, showing that the dynamics remain linear near the center equilibrium point. The more that $\delta\varphi 1$ is varied, the less accurate the trajectories become because the partials matrix is linearized at $P1$.

Next, the phase portrait of the linearized one degree of freedom system orbital resonance solution near the saddle equilibrium point is found. First, the positive trajectories are found by numerically integrating equation (52) with initial conditions at P2 for a time period of 0 to 106 TU and a time period of 106 to 0 TU. Then, the value of δΦ1 is varied from its equilibrium value to +0.00015 with a step size of .00001. Second, the negative trajectories are found by numerically integrating equation (52) with initial conditions at P2 for a time period of 0 to 106 TU and a time period of 106 to 0 TU. Then, the value of δΦ1 is varied from its equilibrium value to −0.00015 with a step size of −0.00001. The positive and negative trajectories are shown in the phase portrait in Figure 11.

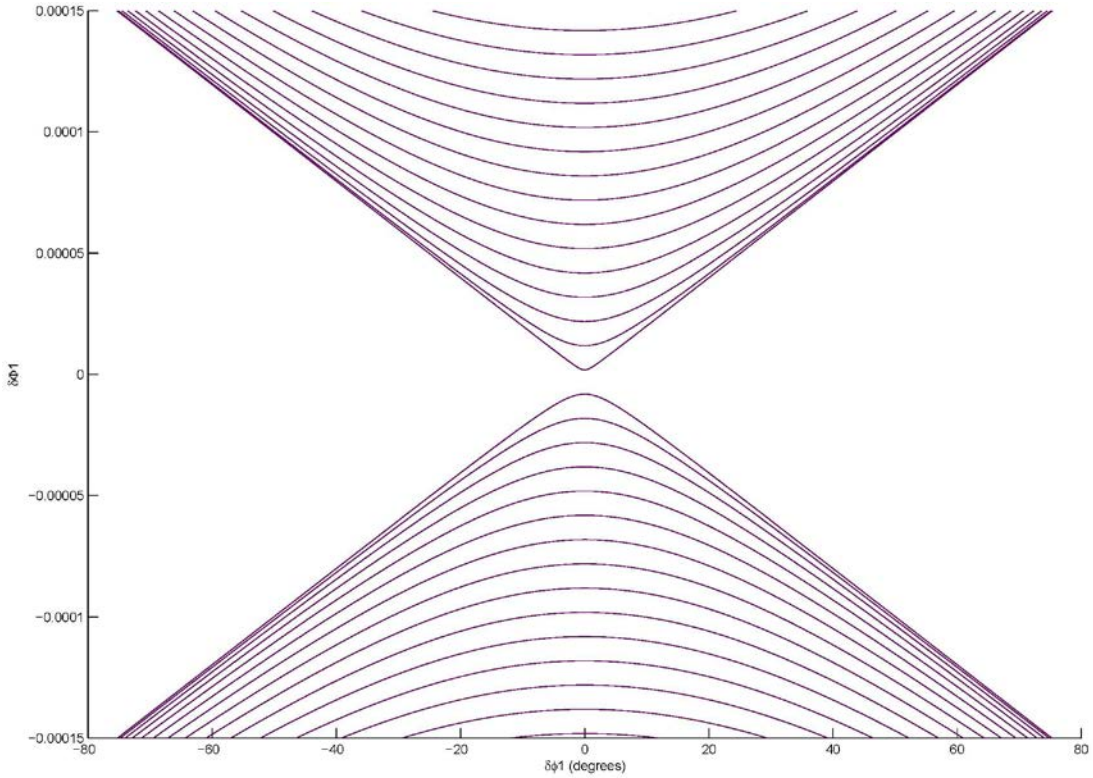

Figure 11. Equations of Variation about Saddle Equilibrium Point Phase Portrait

The direction of motion of the positive trajectories in positive time is from right to left, and the direction of motion of the negative trajectories is from left to right. The farther the trajectories propagate from the equilibrium point, the less accurate the trajectories become because the partials matrix is linearized at P_2. These trajectories continue in a v-shape as time increases and decreases, which differs from the nonlinear dynamics shown in Section 4.6.

GPS Orbit Equations of Motion

Next, the dynamics found in the equations of motion of the orbital resonance solution are explored and compared with the dynamics of the linearized equations of motion. Equations (47) and (48) are the equations of motion for the one degree of freedom orbital resonance solution. The trajectories of the phase space are computed by numerically integrating the equations of motion for 106 time units using ode45 in MATLAB with relative and absolute tolerances of $2.22045 \times 10{-}14$. To create the phase portrait, the initial value of $\varphi 1$ is varied from the center equilibrium point value to 360° and the initial value of $\delta\Phi 1$ is varied from the equilibrium point value to ± 0.0004. Trajectories are computed in positive time from 0 to 106 TU and in negative time from 106 to 0 TU. The resulting trajectories of these numeric integrations are shown in Figure 12.

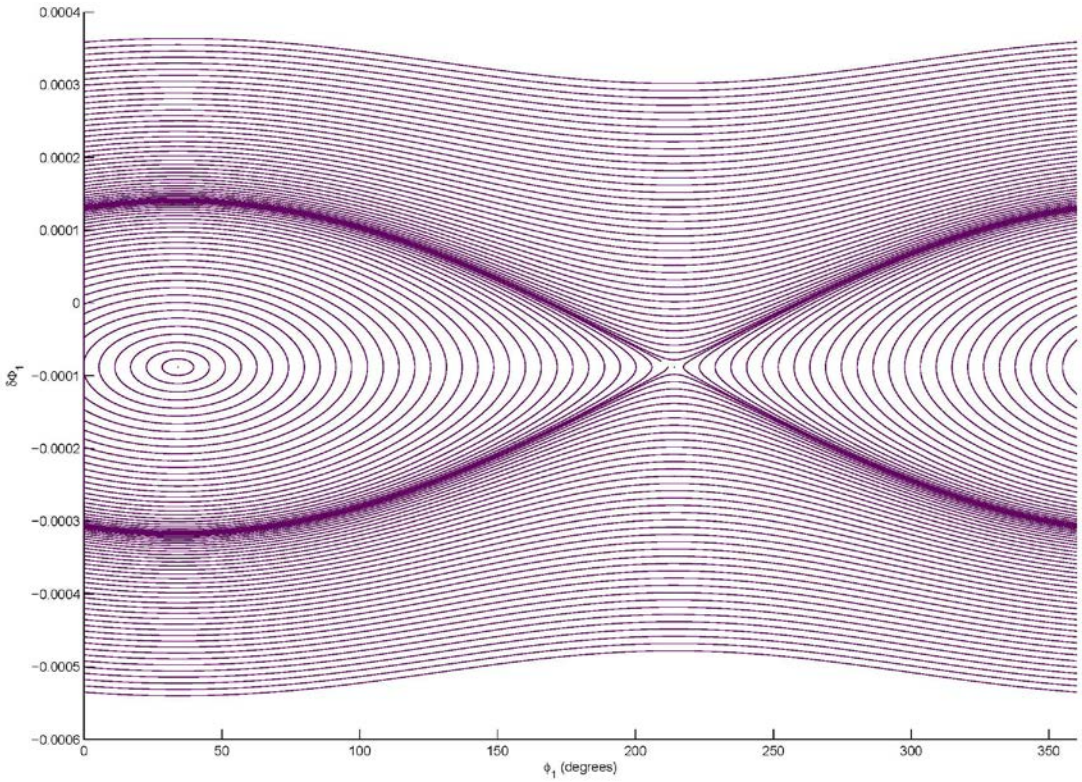

Figure 12. GPS Phase Portrait

In the oval regions of Figure 12, the direction of motion of the trajectories is counterclockwise, which agrees with the linear dynamics. The direction of motion of the trajectories above the oval region is from right to left. The direction of motion of the trajectories below the oval region is from left to right. Next, the equilibrium points P1 and P2 can be identified in the phase portrait. P1 is found at $\varphi 1 \approx 34^\circ$ and has a center equilibrium structure. P2 is found at $\varphi 1 \approx 214^\circ$ and has a saddle equilibrium structure. Similar to the phase portrait shown in Figure 6, the center equilibrium point is located in a libration region and the saddle equilibrium point is located in a chaotic region. Trajectories near the center equilibrium point oscillate about the equilibrium point as time approaches infinity. Trajectories near the saddle point diverge from the point along the unstable eigenvector direction and asymptotically approach the equilibrium point along the stable eigenvector direction as time approaches infinity.

Reach of the 2:1 Resonance

In this section, orbits near the 2:1 resonance are propagated using the orbital resonance solution in order to find the reach of the dynamics due to this resonance. First, the nominal GPS orbit semi-major axis and inclination are translated to Cartesian coordinates, input into the Vinti Solution software, and the Vinti system coordinates are used as initial values for the integrated trajectories using the orbital resonance solution equations of motion. The nominal GPS trajectory is shown in red in Figure 13. Then, the semi-major axis is varied by ±0.1 km and trajectories are found using the above process. The semi-major axis is varied until the trajectory becomes sinusoidal. The sinusoidal trajectories are not affected by the resonance dynamics, and are not included in Figure 13. Finally, the semi-major axis of an orbit directly at the 2:1 resonance is calculated using equation (1) and the trajectory is found using the above process. The 2:1 resonance trajectory is shown in black in Figure 13. The trajectories found using the above process are shown in Figure 13, numbered from top to bottom, and listed in Table 2. All orbits are calculated at an inclination equal to 55° and eccentricity equal to 0, which is the defined nominal GPS orbit.

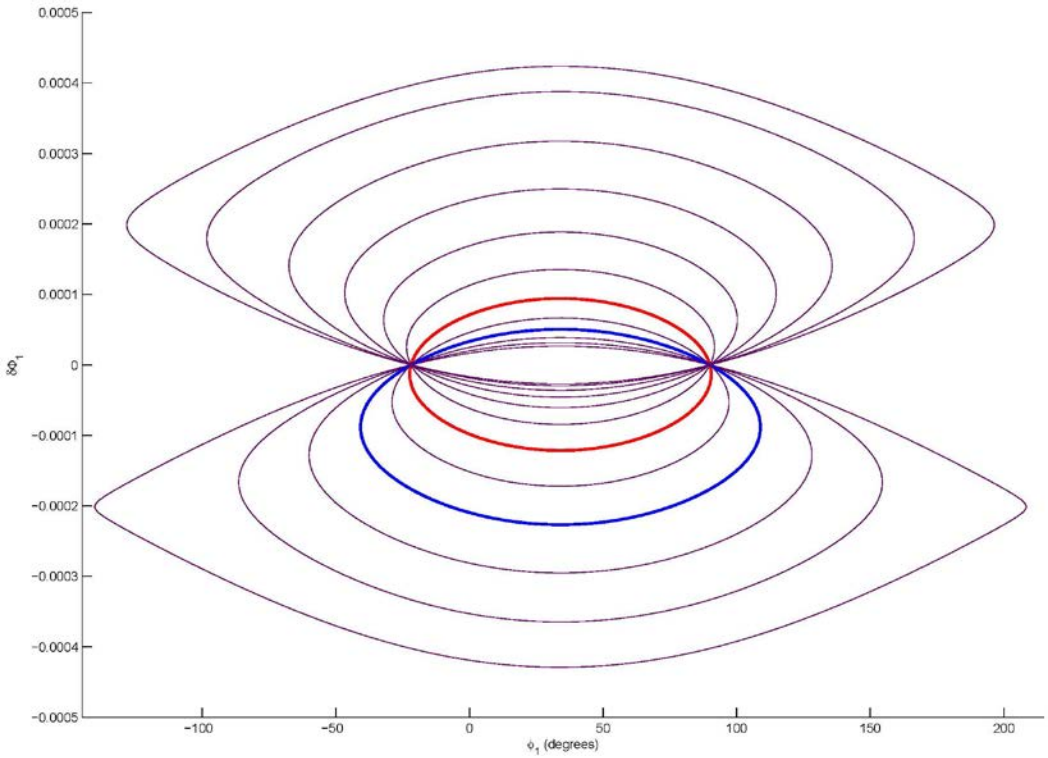

Figure 13. Trajectories near the 2:1 Resonance Phase Portrait

Table 2. Orbits shown in Figure 13

Trajectory	Semi-major Axis (km)	Label
1	26567.210	GPS plus 7.5 km
2	26566.710	GPS plus 7 km
3	26565.710	GPS plus 6 km
4	26564.710	GPS plus 5 km
5	26563.710	GPS plus 4 km
6	26562.710	GPS plus 3 km
7	26561.764	2:1 Resonance
8	26560.710	GPS plus 1 km
9	26559.710	GPS
10	26558.710	GPS minus 1 km
11	26557.710	GPS minus 2 km
12	26556.810	GPS minus 2.9 km

The reach of the dynamics due to the 2:1 resonance is found to be −5.0 km to +5.4 km in semi-major

axis, when rounded to the nearest tenth decimal place. The nominal GPS orbit happens to be located within this range, which means that it is affected by 2:1 resonance dynamics. The reason that the reach of the 2:1 resonance is not equal in the positive and negative directions is because the period of the orbit squared is proportional to the semi-major axis cubed. Thus, a linear change in semi- major axis will result in a nonlinear change in period. Therefore, the reach of the dynamics due to orbital resonance is asymmetric in semi-major axis.

The reach of the dynamics due to resonance is explored further by producing truth orbits in STK and translating the truth orbits to the Vinti system.

Validation using GPS Truth Orbits

In this section, the truth orbits of GPS satellites are produced in STK and the dynamics are compared with those found in the orbital resonance solution.

Seven GPS satellites are chosen that orbit in the same orbital plane with a right ascension of the ascending node equal to approximately 180°. These seven GPS TLE files are input into STK and converted to classical orbital elements (COEs), which are reported in Table 3.

Table 3. COEs found in STK

Satellite Name	Semi-major Axis (km)	Eccentricity	Inclination (deg)	RAAN (deg)	Argument of Perigee (deg)	True Anomaly (deg)
GPS-BIIA-10	26558.648198	0.011391	54.211	186.589	11.500	246.447
GPS-BIIF-11	26844.160534	0.000802	54.953	181.828	194.808	260.103
GPS-BIIF-08	26558.580289	0.000365	54.930	182.047	182.880	50.014
GPS-BIIR-04	26559.717827	0.005009	53.045	177.495	74.589	345.753
GPS-BIIR-07	26561.779713	0.016388	52.971	180.478	249.998	117.820
GPS-BIIR-10	26576.090729	0.007501	52.847	180.522	244.090	84.470
GPS-BIIRM-08	26559.176516	0.004564	54.193	181.486	27.180	74.488

These seven orbits are then propagated in STK for ten years with a step size of 600 seconds. In STK, the Earth's gravity model is defined by World Geodetic System 1984 (WGS84) and the Earth's Gravitational Model 1996 (GM96). WGS84 models the Earth's gravity on a geoid relative to a reference ellipsoid and was established in 1984 [29]. GM96 approximates the geopotential of the Earth using spherical harmonics and was developed in 1996 [30]. The gravity model used to produce the truth orbits is WGS84 GM96 with a maximum degree of two, a maximum order of two, and no solid tides. Drag, solar radiation pressure, and third body gravity effects are not used in the propagation. This force model best simulates local action and angle coordinates of the Vinti system used to derive the orbital resonance solution. The propagator used is the high precision orbit propagator (HPOP) with RKF 7(8) integration. The relative error tolerance is specified as 10^{-13}.

Reports are generated for the inertial position and velocity of the seven orbits for ten years. The position and velocity values from the report are then translated to Vinti coordinates and momenta using the Vinti solution software provided by Wiesel.

The resulting trajectories of the seven coplanar GPS satellites in the Vinti system are shown in Figure 14.

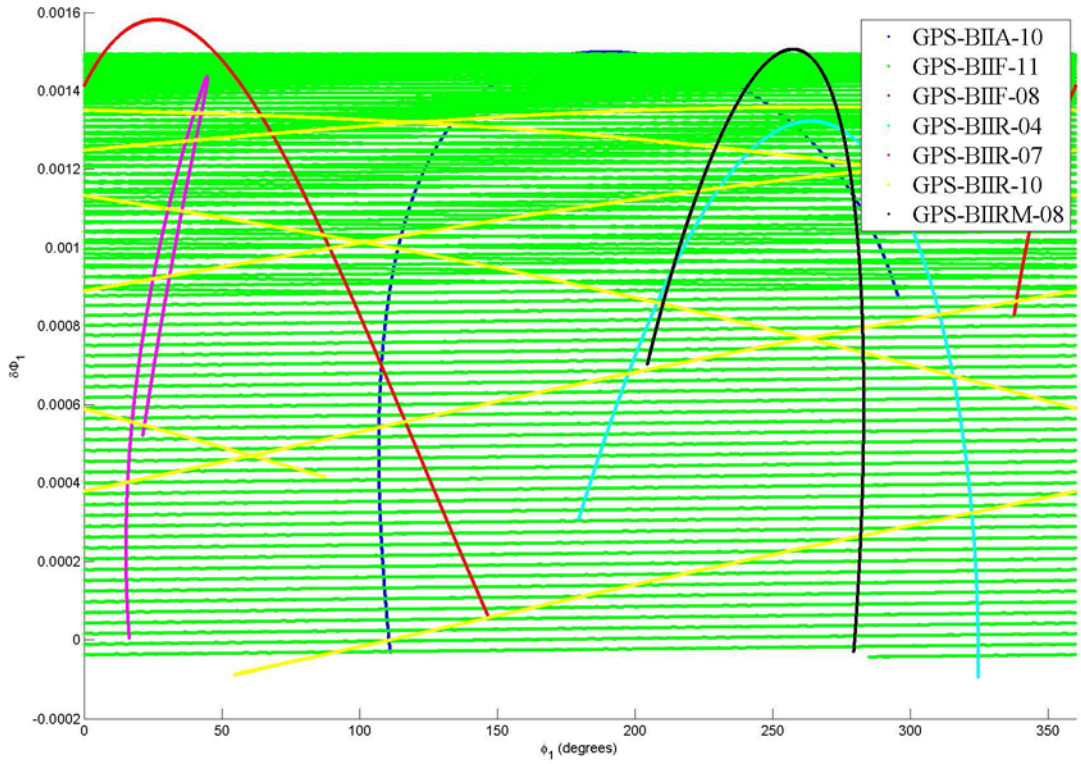

Figure 14. Truth Orbits of 7 GPS Satellites Propagated for 10 Years

Figure 14 shows one GPS satellite, GPS-BIIF-11, shown in green, displaying dras- tically different dynamics than the rest of the satellites. The direction of motion of this satellite is from left to right and the momentum, $\delta\Phi_1$, steadily decreases as time increases. The GPS-BIIF-11 satellite has an initial semi-major axis of 26844.160534 km, which is well outside of the reach of the resonance shown in Section 4.7. This orbit is removed to analyze the six other orbits, which are closer to the resonance.

Figure 15 shows the ten year trajectories of the six GPS satellites in the same orbital plane located closest to the resonance.

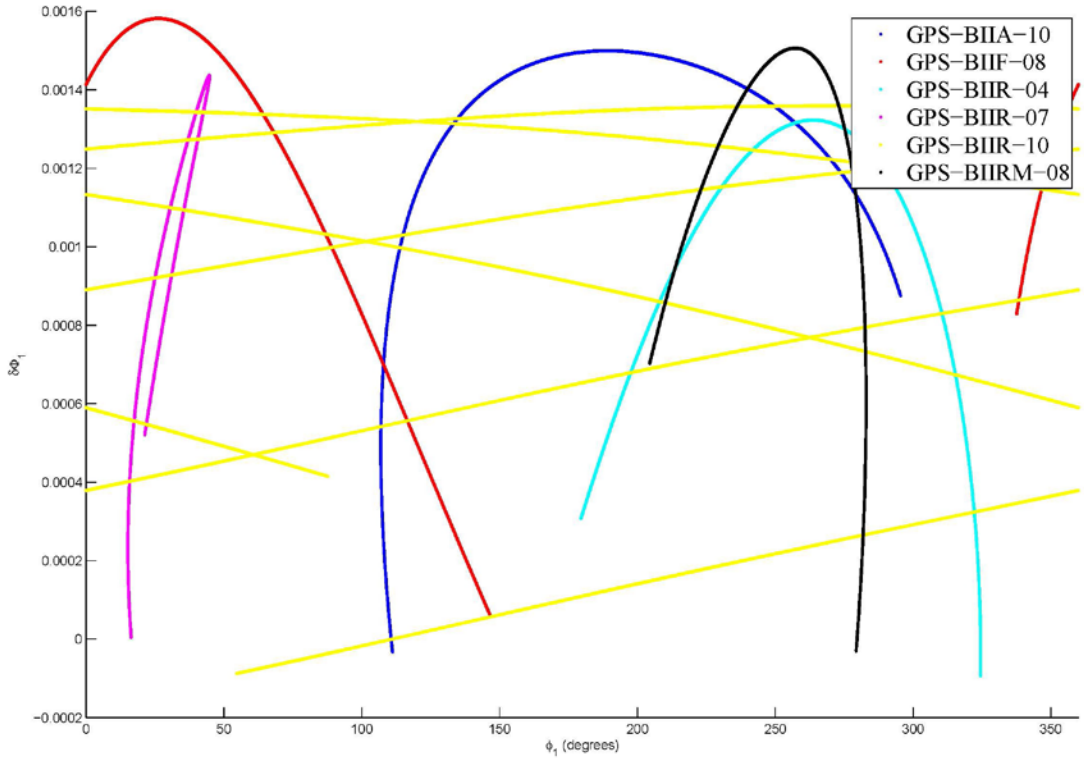

Figure 15. Truth Orbits of 6 Coplanar GPS Satellites, Propagated for 10 Years

From these six trajectories, one satellite shows unique dynamics. The GPS-BIIR- 10 satellite, shown in yellow, with a semi-major axis of 26576.090729 km is slightly outside of the reach of the resonance, but its dynamics can be observed in Figure 12, the GPS phase portrait. Since the momentum, $\delta\Phi_1$, of GPS-BIIR-10 is increasing and decreasing as φ_1 increases and the direction of motion is from left to right, it is located just below the libration region of the phase portrait. This region appears wavy in the phase portrait because the momentum oscillates as time increases. The semi-major axis of GPS-BIIR-10 is just outside of the reach of the resonance, so it can be removed to further analyze the dynamics near the resonance.
Figure 16 shows the ten year trajectories of the five GPS satellites in the same orbital plane located within the reach of the resonance.

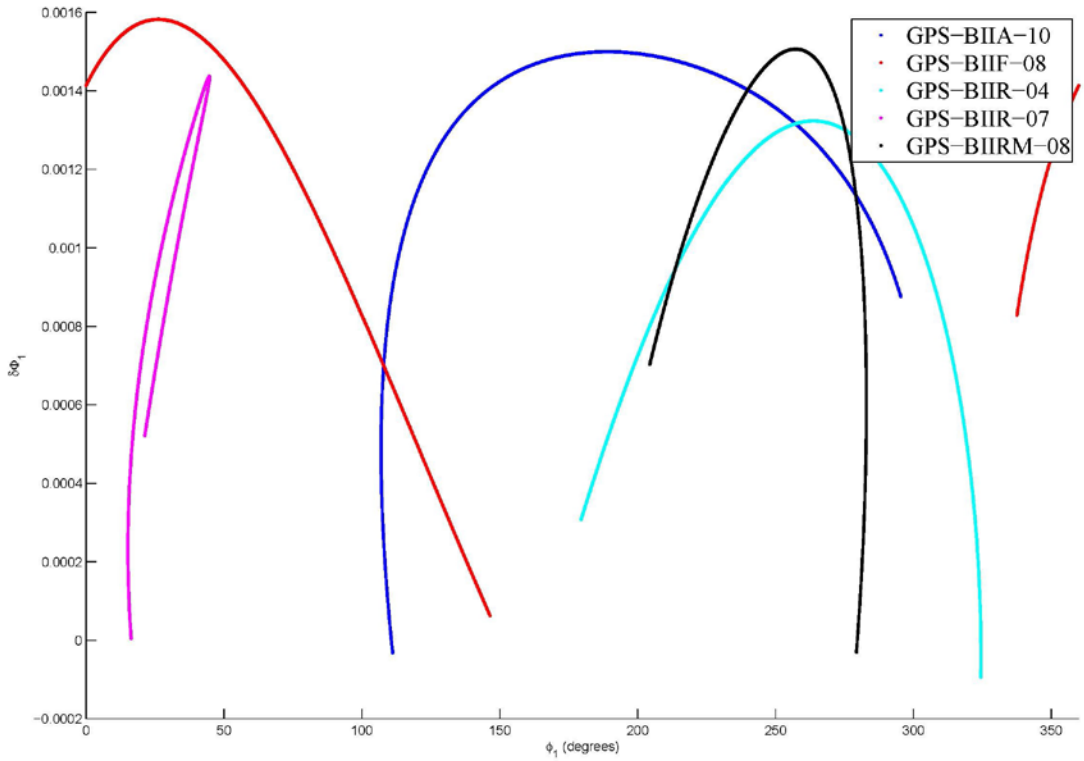

Figure 16. Truth Orbits of 5 Coplanar GPS Satellites within 2:1 Resonance, Propagated for 10 Years

All five of the satellites in Figure 16 have arc-shaped trajectories. These shapes resemble the trajectories found in the upper half of the libration region of the phase portrait. All of these satellites have semi-major axes within reach of the resonance, and the trajectories produced in STK clearly show the effects of the resonance. GPS- BIIA-10 and GPS-BIIR-07 have directions of motion from left to right. GPS-BIIF- 08, GPS-BIIR-04, and GPS-BIIRM-08 have directions of motion from right to left. These five GPS satellites tend to follow the dynamics found in the upper half of the libration region of the phase portrait. These trajectories show that the GPS satellites with semi-major axes within reach of the dynamics due to the resonance are affected by the resonance for long time periods.

The libration region of the phase portrait contains counter-clockwise trajectories, which is consistent with the three GPS arcs moving from right to left. However, the two left to right arcs are inconsistent with the dynamics of the phase portrait. A possible explanation of these dynamics is that the satellites may be influenced by the dynamics of nearby resonances. In the research presented in Section 2.4, the interactions of multiple resonances were found to result in highly nonlinear motions. This same explanation could also be causing the nonlinear motions of the GPS satellites in Figure 16.

Also, the accuracy of these trajectories is limited by the precision of the initial conditions. The TLE data sets are translated to COEs in STK, but the numerical accuracy of these initial condition is limited to six decimal places in semi-major axis and eccentricity, while the inclination, RAAN, argument of perigee, and true anomaly are limited to three decimal places. When integrating for long time periods, such as decades, accurate initial conditions are essential. Since the initial conditions are limited in accuracy, this is a source of error for the long propagations performed in STK.

If any of the satellites are located near the chaotic region of the phase space, they are even more sensitive to initial conditions. One of the satellites, the GPS-BIIR-07, shown in magenta, appears to be near one of these chaotic regions. GPS-BIIR-07 has a semi-major axis of 26561.779713 km, which is very near the 2:1 resonant orbit semi-major axis of 26561.764 km. Since its motion changes quickly at approximately $\varphi 1 = 45^\circ$, its orbit is propagated in STK for twenty years to examine long-term behavior. This propagation is shown in Figure 17.

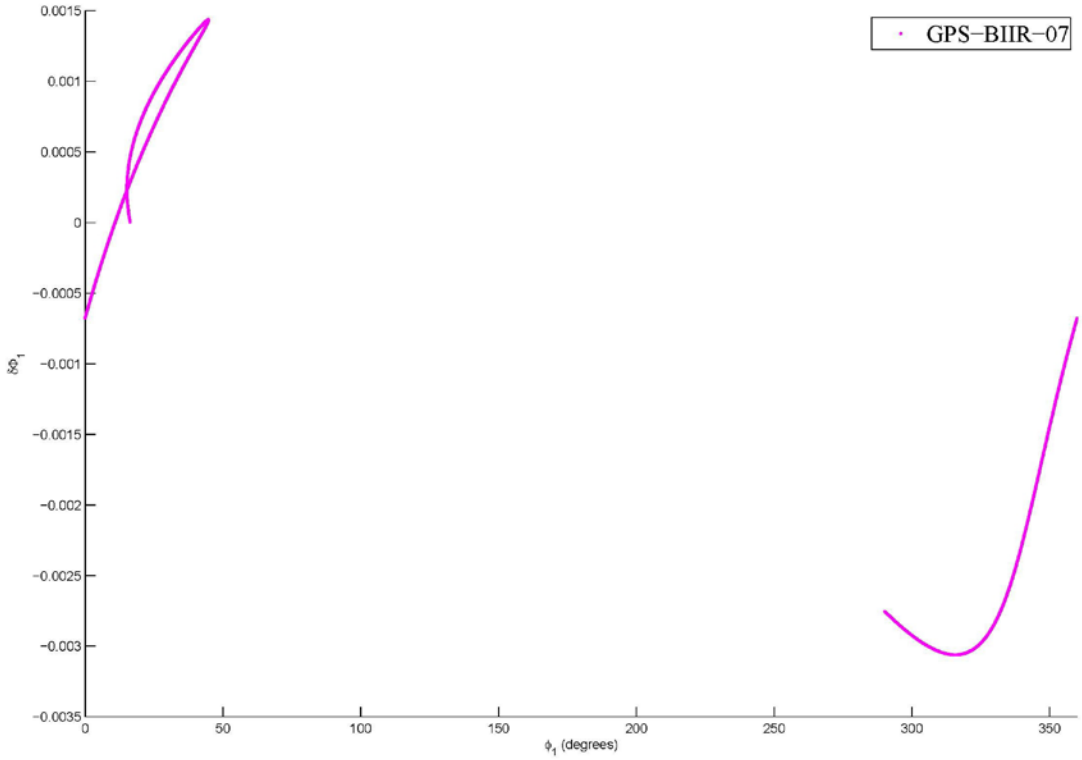

Figure 17. Truth Orbit of 1 GPS Satellite within 2:1 Resonance, Propagated for 20 Years

The trajectory in Figure 17 starts at φ1 = 16◦ and ends at φ1 = 290◦. At the beginning of the trajectory, the satellite appears to be approaching a chaotic region because the dynamics rapidly change. Since the resonance variable is bounded between 0◦ and 360◦, the trajectory jumps from the left side to the right side of the plot in Figure 17. By the end of the trajectory, the trajectory displays the dynamics found in the lower half of the libration region of the phase space.

One issue with numerically propagating in STK is that as time increases, the predictions become less accurate due to the numerical accuracy of the propagator. For propagations of ten to twenty years, the numerical accuracy appears good enough to show the long-term effects of the dynamics due to orbital resonance.

CONCLUSION

Conclusions

Operations in space require accurate orbit predictions using orbit propagators. Current orbit propagators use SGP4, which utilizes the two body problem plus perturbation theory. The Vinti Solution offers a more accurate solution than the two body problem. Unfortunately, small divisors appear in the perturbative terms of the Vinti Solution near orbital resonances, leading to large terms and inaccurate orbit predictions. The research in this thesis provides a solution to avoid the large terms that appear near orbital resonances. It is referred to as the orbital resonance solution. Numerous resonant orbits are used for critical satellite systems in GEO, MEO, and LEO including SBIRS, GPS, and Landsat. In order to keep these satellites safe from collision and to make accurate orbit predictions for advanced space operations, a highly accurate model is required. The Vinti Solution, when corrected for orbital resonances, offers a more accurate method for predicting satellite locations. A method to correct for orbital resonances is offered in this thesis. The scope of this research focuses on orbital resonances due to the gravity field. It only applies to Earth orbiting satellites. The solution provided in this thesis applies to all orbital resonances from the 1:1 to 16:1 resonances. The truth orbits used to analyze the effectiveness of the orbital resonance solution are produced using STK with an error tolerance of 10^{-13}. Numerical analyses are performed using MATLAB with an error tolerance of 2.22045×10^{-14}, which inherently limits the accuracy of the integrations. Also, Vinti Solution software provided by Dr. Wiesel is utilized to change from Cartesian coordinates to Vinti system coordinates and momentum.

The Literature Review provides theory and research of the background knowledge necessary to understand the thesis. First, the Vinti Solution is explained because the orbital resonance solution provided in this thesis is designed to be used in conjunction with a numerical model of the Vinti Solution. Second, orbital resonances are defined because they are poorly modeled in the Vinti Solution, leading to the need for this research. Third, the findings of research on resonances found in the GPS constellation are summarized. Fourth, research on resonances in the KAM theorem is presented. Fifth, classical mechanics is explained because it provides the foundational concepts used to develop the Vinti Solution and the orbital resonance solution. Finally, trans- formation theory is described because it is used to derive the equations of motion for the orbital resonance solution.

In the Methodology, the orbital resonance solution is derived. The resonant terms from the Hamiltonian of the Vinti Solution are identified, transformation theory is applied to derive the new Hamiltonian, and Hamilton's canonical equations of motion are applied to find the equations of motion of the orbital resonance solution.

In order to analyze the orbital resonance solution, a case study of the GPS constellation is applied because it is located near the 2:1 resonance. A nominal GPS orbit is defined and translated into Vinti system coordinates and momenta.

The orbital resonance solution is then reduced to a one degree of freedom system, resulting in two equations of motion. The coordinate of this system is φ_1, the resonant term. The momentum of this system is Φ_1, the associated momentum of the resonant term.

The equilibrium points of the one degree of freedom orbital resonance solution are found for the nominal GPS orbit. Two equilibrium points are found: one marginally stable center point and one unstable saddle point. The imaginary value of the stable eigenvalue defines the system frequency, which is found to be approximately 44 degrees/year. This means that the dynamics due to orbital resonances can only be observed for long time periods. Unfortunately, integrating for long time periods increases the magnitude of numerical errors. The linear dynamics near the equilibrium points are examined. In the vicinity of the stable equilibrium point, trajectories are found to oscillate around the point. In the vicinity of the unstable equilibrium point, trajectories are found to quickly diverge from the point.

The nonlinear one degree of freedom equations of motion of the orbital resonance solution are applied to the nominal GPS orbit. These equations are numerically integrated to create the phase portrait of the GPS satellite. The equilibrium points are easily identified within the phase portrait. Trajectories near the center equilibrium point encircle the point in the libration region. Trajectories near the saddle point diverge from the point along the unstable eigenvector direction and asymptotically approach the equilibrium point along the stable eigenvector direction.

Various orbits near the 2:1 resonance are examined to determine the reach of the 2:1 resonance. When

measured in change in semi-major axis and rounded to the nearest tenth decimal place, the reach of the dynamics due to the 2:1 resonance is found to be −5.0 km to +5.4 km.

Truth orbits are produced in STK to analyze the accuracy of the orbital resonance solution. Seven GPS satellites within the same orbital plane or chosen and propagated for ten years. The accuracy of these truth orbits is limited by the accuracy of the initial classical orbital elements used. One of the satellites is found to be outside of the reach of the 2:1 resonance and the dynamics are not influenced by the resonance. Another satellite is found to be just outside of the reach of the resonance and its momentum oscillates for all time. The remaining five satellites are found to be within reach of the resonance and appear to be in the libration region of the phase space because they make arcing motions. However, some of these arcs move in the opposite direction of the phase portrait. This may be due to influences of nearby resonances. One satellite happens to be very near the 2:1 resonance. When propagated for 20 years, it appears to be influenced by chaotic motion and later settles into an arcing motion. All five of the GPS satellites within reach of the resonance are clearly affected by the dynamics due to resonance.

The main limitation of this research is found to be evident in the validation using the truth orbits. In the orbital resonance solution, only one resonance can be modeled at a time. However, the true dynamics of the orbit are affected by multiple interacting frequencies, which results in highly nonlinear motion. This highly nonlinear motion is not evidenced by the orbital resonance solution, but can be seen in the truth orbits that contradict the orbital resonance phase portrait.

The first main conclusion of this research is that transformation theory offers a valid method of avoiding small divisors near orbital resonances. Through the use of transformation theory, the orbital resonance solution is found, which can accurately model the dynamics due to resonances in the Vinti Solution. Previously, this was not possible due to small divisors. The orbital resonance solution is the most significant and novel contribution of this research.

The second conclusion of this research is that the phase space of a nominal GPS orbit contains a libration region and a chaotic region due to orbital resonance. The phase portrait of the nominal GPS orbit has a “center” equilibrium point within the libration region and a “saddle” equilibrium point within the chaotic region.

The third main conclusion is that the reach of the 2:1 resonance is found to be -5.0 to +5.4 km in semi-major axis.

The fourth main conclusion is that GPS truth orbits confirm that resonance dynamics exist for orbits within reach of the 2:1 resonance. These truth orbits validate that the orbital resonance solution is a valid method for modeling resonance perturbative terms in the Vinti solution.

Recommendations for Future Research

Several aspects of this research could benefit from further analysis due to the limitations of the problem.

First, the dynamics near resonances other than the 2:1 resonance could be explored. The phase portraits showing dynamics near these resonances could be produced. Also, the reach of these resonances could be explored to see the range of semi-major axes that are affected by resonance dynamics. The 1:1 resonance, also known as GEO, is utilized for numerous high-cost space systems and could benefit from an analysis of the dynamics due to resonance. Also, the numerous resonances found in LEO could benefit from this research since these orbits are highly populated due to their proximity to Earth.

Second, further research could explore an alternative change of coordinates, resulting in an alternative orbital resonance solution. It is possible that a different set of coordinates could offer a more accurate way of representing the Vinti system while still avoiding the small divisors.

Third, the chaotic region of the phase space appears to be highly sensitive when modeled numerically. This region could benefit from further exploration in future research.

Finally, the main limitation with the orbital resonance solution provided in this thesis is that only one resonance can be modeled at a time. The actual orbital dynamics are influenced by multiple interacting resonances which result in highly nonlinear motions. Future research could develop a model to incorporate the interacting resonances to gain greater insight into the phase space of orbits near resonances in the Vinti Solution.

BIBLIOGRAPHY

1. "USSTRATCOM Space Control and Space Surveillance," U.S. Strategic Command, January 2014, available at https://www.stratcom.mil/factsheets/11/Space_Control_and_Space_Surveillance/.

2. "Simplified perturbations models," Wikimedia Foundation, Inc., December 2014, available at https://en.wikipedia.org/wiki/Simplified_perturbations_models.

3. W. E. Wiesel, September 2015, personal communication.

4. J. P. Vinti, "New Method of Solution for Unretarded Satellite Orbits," Journal of Research of the National Bureau of Standards, vol. 62B, no. 2, 1959.

5. "SPACE BASED INFRARED SYSTEM (SBIRS)," Los Angeles Air Force Base, May 2015, available at http://www.losangeles.af.mil/library/factsheets/factsheet.asp?id=22323.

6. "Earth," Wikimedia Foundation, Inc., August 2015, available at https://en.wikipedia.org/wiki/Earth.

7. "Low Earth orbit," Wikimedia Foundation, Inc., June 2015, available at https://en.wikipedia.org/wiki/Earth.

8. "Medium Earth orbit," Wikimedia Foundation, Inc., May 2015, available at https://en.wikipedia.org/wiki/Medium_Earth_orbit.

9. "GPS Applications," National Coordination Office for Space-Based Position, Navigation, and Timing, November 2014, available at http://www.gps.gov/applications/.

10. "Landsat Project Description," September 2013, available at http://landsat.usgs.gov/about_project_descriptions.php.

11. W. E. Wiesel, "Low Eccentricity Earth Satellite KAM Tori," report submitted for publication in Journal of the Astronautical Sciences. Department of Aeronautics and Astronautics, Air Force Institute of Technology, Wright Patterson AFB, OH, 2015.

12. "The Persistent Problem of Orbital Debris," Secure World Foundation, February 2015, available at http://swfound.org/space-sustainability-101/the-persistent-problem-of-orbital-debris/.

13. NASA, "Monthly Effective Mass of Objects in Earth Orbit by Region," Orbital Debris Quarterly News, vol. 19, no. 1, p. 9, 2015.

14. "ode45," The MathWorks, Inc., 2015, available at http://www.mathworks.com/help/matlab/ref/ode45.html.

15. "MATLAB," Wikimedia Foundation, Inc., July 2015, available at https://en.wikipedia.org/wiki/MATLAB.

16. "Systems Tool Kit," Wikimedia Foundation, Inc., April 2015, available at https://en.wikipedia.org/wiki/Systems_Tool_Kit.

17. W. E. Wiesel, "Numerical Solution to Vinti's Problem," Journal of Guidance, Control, and Dynamics, vol. 0, no. 0, 2014, doi: 10.2514/1.G000661.

18. H. Poincaré, Les Methodes Nouvelles de la Mecanique Celeste. New York: Dover Publications, Inc., 1957, vol. 2.

19. B. V. Chirikov, "A Universal Instability of Many-Dimensional Oscillator Systems," Physics Reports,

vol. 52, no. 5, pp. 263 – 379, 1979. [Online]. Available: http://www.sciencedirect.com/science/article/pii/0370157379900231

20. W. E. Wiesel, Modern Astrodynamics, 2nd ed. Beavercreek, OH: Aphelion Press, 2010.

21. J. Sampaio, A. Neto, S. Fernandes, R. V. de Moraes, and M. Terra, "Artificial satellites orbits in 2:1 resonance: GPS constellation," Acta Astronautica, vol. 81, no. 2, pp. 623 – 634, 2012. [Online]. Available: http://www.sciencedirect.com/science/article/pii/S0094576512003359

22. "Kolmogorov-Arnold-Moser theorem," Wikimedia Foundation, Inc., June 2015, available at https://en.wikipedia.org/wiki/Kolmogorov-Arnold-Moser_theorem.

23. "Kolmogorov-Arnold-Moser theory," Prof. James Meiss, Applied Mathematics University of Colorado, Boulder, CO, USA, October 2011, available at http://www.scholarpedia.org/article/Kolmogorov-Arnold-Moser_theory.

24. R. E. B. III, "Orbital Tori Construction Using Trajectory Following Spectral Methods," Ph.D. dissertation, Air Force Institute of Technology, 2010.

25. W. E. Wiesel, Spaceflight Dynamics, 3rd ed. Beavercreek, OH: Aphelion Press, 2010.

26. D. T. Greenwood, Classical Dynamics. New York: Dover Publications, Inc., 1977.

27. L. Meirovitch, Methods of Analytical Dynamics. New York: Dover Publications, Inc., 2003.

28. "Global Positioning System Standard Positioning Service Performance Standard," National Coordination Office for Space-Based Positioning, Navigation, and Timing, September 2008, available at http://www.gps.gov/technical/ps/2008-SPS-performance-standard.pdf.

29. "World Geodetic System," Wikimedia Foundation, Inc., February 2016, available at https://en.wikipedia.org/wiki/World_Geodetic_System.

30. "EGM96," Wikimedia Foundation, Inc., January 2016, available at https://en.wikipedia.org/wiki/EGM96.

31. "GPS-OPS," Celestrak, December 2015, available at http://www.celestrak.com/NORAD/elements/gps-ops.txt.